Report no. 00/18

A spectral Petrov-Galerkin formulation for pipe flow I: Linear stability and transient growth

A. Meseguer
L. N. Trefethen

Oxford University Computing Laboratory
Numerical Analysis Group
Wolfson Building
Parks Road
Oxford, England OX1 3QD

September, 2000

Abstract

A spectral Petrov-Galerkin scheme for the numerical approximation of flow in a circular pipe is presented. The mathematical formulation is presented in detail focusing on the analyticity of solenoidal vector fields used for the approximation of the flow. A comprehensive study of linear stability is reported for axisymmetric, non-axisymmetric, streamwise dependent and streamwise independent perturbations . The scheme provides spectral accuracy in all cases studied and the numerical results are in agreement with former works. A parametric exploration of pseudospectra and transient growth has been carried out for the aforementioned cases.

1 The pipe flow problem

The pipe or Hagen-Poiseuille flow problem is the problem of fluid motion in an infinite circular pipe, whose radius we will call a. The fluid is driven axially by an uniform external pressure gradient $\Pi_0 \hat{z}$ in the direction of the axis of the pipe (Batchelor, 1967). The behaviour of the fluid is governed by the incompressible Navier-Stokes equations:

$$\partial_t \mathbf{v} + (\mathbf{v}\cdot\nabla)\mathbf{v} = -\frac{\Pi_0}{\rho}\hat{z} - \nabla p + \nu\Delta\mathbf{v} \tag{1.1}$$

$$\nabla\cdot\mathbf{v} = 0, \tag{1.2}$$

where $\mathbf{v}$ is the *velocity* vector field which must be zero over the cylinder wall, p is the *reduced pressure*, ρ is the *density* of the fluid and $\nu = \mu/\rho$ is the *kinematic viscosity*, μ being the *dynamic viscosity*. Equations (1.1-1.2) can be rewritten in cylindrical coordinates (r,θ,z) as follows:

$$\partial_t u + u\partial_r u + \frac{v}{r}\partial_\theta u + w\partial_z u - \frac{v^2}{r} = -\partial_r p + \nu\Delta u - \frac{2}{r^2}\partial_\theta v - \frac{u}{r^2}, \tag{1.3}$$

$$\partial_t v + u\partial_r v + \frac{v}{r}\partial_\theta v + w\partial_z v + \frac{uv}{r} = -\frac{1}{r}\partial_\theta p + \nu\Delta v + \frac{2}{r^2}\partial_\theta u - \frac{v}{r^2}, \tag{1.4}$$

$$\partial_t w + u\partial_r w + \frac{v}{r}\partial_\theta w + w\partial_z w = -\frac{\Pi_0}{\rho} + \nu\Delta w, \tag{1.5}$$

$$\partial_r u + \frac{1}{r}\partial_\theta v + \partial_z w + \frac{u}{r} = 0, \tag{1.6}$$

$$(u,v,w) = \mathbf{0} \quad \text{for} \quad r = a, \tag{1.7}$$

where u, v and w are the radial, azimuthal and axial components of the velocity vector field $\mathbf{v}$, respectively. In these equations, Δ stands for the Laplacian operator in cylindrical coordinates,

$$\Delta = \partial_r^2 + \frac{1}{r}\partial_r + \frac{1}{r^2}\partial_\theta^2 + \partial_z^2. \tag{1.8}$$

By assuming certain symmetries we can derive analytically a basic solution of the equations (1.3-1.7). The basic flow can be derived assuming a steady solution independent of the axial and azimuthal coordinates (z,θ). In addition, the flow field is assumed to be oriented in the direction $\hat{z}$ of the axis of the pipe. In other words, the basic flow $\mathbf{v}_B = (u_B, v_B, w_B)$ satisfies

$$u_B = v_B = \partial_t w_B = \partial_\theta w_B = \partial_z w_B = 0. \tag{1.9}$$

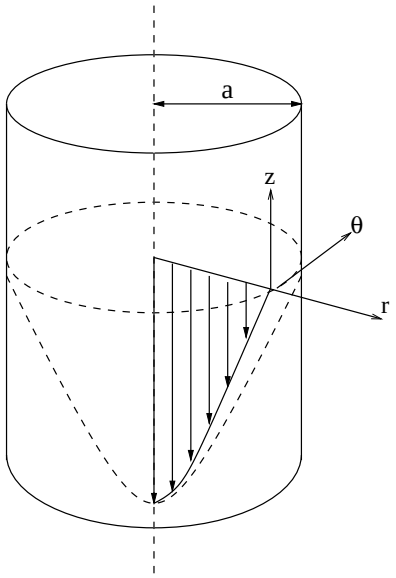

Figure 1: Hagen-Poiseuille flow. The basic flow $\mathbf{v}_B(r)$ is driven by the axial pressure gradient $\Pi_0 \hat{z}$.

The basic solution is (1.3-1.6) and (1.9) is found to be

$$w_B(r) = -\frac{\Pi_0}{4\rho\nu}\left[1 - \left(\frac{r}{a}\right)^2\right], \quad \partial_r p = 0, \quad \partial_\theta p = 0, \tag{1.10}$$

which is an axisymmetric parabolic velocity profile usually termed *Hagen-Poiseuille* flow (Batchelor, 1967). The velocity of the fluid attains a maximum value $U_{CL} = -\Pi_0/4\rho\nu$ at the *centerline* or axis of the cylinder. A geometrical sketch of the Hagen-Poiseuille flow is given in figure 1.

2 Linear Stability

In this section, we suppose that the basic flow is perturbed by an infinitesimal solenoidal velocity field which must vanish over the cylinder wall,

$$\mathbf{v}(r,\theta,z,t) = \mathbf{v}_B(r) + \mathbf{u}(r,\theta,z,t), \quad \nabla\cdot\mathbf{u} = 0, \quad \mathbf{u}_{r=a} = 0, \tag{2.1}$$

and a perturbation pressure field

$$p(r,\theta,z,t) = p_B(r) + q(r,\theta,z,t), \tag{2.2}$$

where $\mathbf{u}$ and q are the velocity and reduced pressure perturbation fields, respectively. On introducing $\mathbf{v}$ in (1.1– 1.2), we obtain the equation for the perturbation fields

$$\partial_t\mathbf{u} = -\nabla q + \nu\Delta\mathbf{u} - (\mathbf{v}_B\cdot\nabla)\mathbf{u} - (\mathbf{u}\cdot\nabla)\mathbf{v}_B - (\mathbf{u}\cdot\nabla)\mathbf{u}. \tag{2.3}$$

Neglecting the nonlinear term $(\mathbf{u}\cdot\nabla)\mathbf{u}$, we obtain the linearized Navier-Stokes equations for the perturbation,

$$\partial_t\mathbf{u} = -\nabla q + \nu\Delta\mathbf{u} - (\mathbf{v}_B\cdot\nabla)\mathbf{u} - (\mathbf{u}\cdot\nabla)\mathbf{v}_B. \tag{2.4}$$

Henceforth, all variables will be rendered dimensionless using a and U_{CL} as *space* and *velocity* units, respectively. This nondimensionalization procedure leads to the so called *advective time* $\tau_a = a/U_{CL}$. In other words, a fluid particle initially located at the axis of the pipe is advected downstream by the basic flow one pipe radius a after a time τ_a. The nondimensionalization of the variables and the differential operators is summarized as follows:

$$[a] = L, \quad [\frac{a}{U_{CL}}] = T, \tag{2.5}$$

$$r = ar^*, \quad z = az^*, \quad \mathbf{u} = U_{CL}\mathbf{u}^*, \quad \mathbf{v}_B = U_{CL}\mathbf{v}_B^* = U_{CL}(1 - r^{*2}), \quad q = U_{CL}^2 q^*, \tag{2.6}$$

$$\partial_t = \frac{U_{CL}}{a}\partial_t^*, \quad \nabla = \frac{1}{a}\nabla^*, \quad \Delta = \frac{1}{a^2}\Delta^*, \tag{2.7}$$

where $*$ stands for dimensionless variables and operators. Substitution of these previous quantities in (2.4) leads to the nondimensional equation of the perturbation

$$\partial_t \mathbf{u} = -\nabla q + \frac{1}{\mathrm{Re}}\Delta\mathbf{u} - (\mathbf{v}_B \cdot \nabla)\mathbf{u} - (\mathbf{u} \cdot \nabla)\mathbf{v}_B, \tag{2.8}$$

where we have dropped the $*$ symbols for simplicity and the *Reynolds number* Re is defined by

$$\mathrm{Re} = \frac{aU_{CL}}{\nu}.$$

Fourier analysis ensures that without loss of generality we may assume integer periodicity in the azimuthal coordinate θ and real periodicity in the axial coordinate z. Thus, we write

$$\mathbf{v}(r, \theta, z, t) = \mathbf{v}_B(r) + \mathrm{e}^{\mathrm{i}(n\theta + kz) + \lambda t}\mathbf{u}(r), \tag{2.9}$$

$$p(r, \theta, z, t) = p_B(r, z) + p'(r)\mathrm{e}^{\mathrm{i}(n\theta + kz) + \lambda t}, \tag{2.10}$$

where $n \in \mathbb{N}$, $k \in \mathbb{R}$, $\lambda \in \mathbb{C}$. Since λ is in general a complex number, we are not assuming periodicity in time. The boundary conditions for $\mathbf{u}$ are

$$\mathbf{u}(0) \text{ bounded}, \quad \mathbf{u}(1) = \mathbf{0} \tag{2.11}$$

On introducing (2.9) and (2.10) into (2.8), we obtain the following eigenvalue problem:

$$\lambda\mathbf{u} = -\nabla p' + \frac{1}{\mathrm{Re}}\Delta\mathbf{u} - \mathbf{v}_B \cdot \nabla\mathbf{u} - \mathbf{u} \cdot \nabla\mathbf{v}_B, \tag{2.12}$$

where $\nabla p'$ is the perturbation of the reduced pressure gradient. In addition, the perturbation field must satisfy the solenoidal condition

$$\nabla \cdot [\mathrm{e}^{\mathrm{i}(n\theta + kz) + \lambda t}\mathbf{u}(r)] = 0. \tag{2.13}$$

In order to solve (2.12)-(2.13) numerically, we will utilize a spatial discretization with a basis of vector fields which satisfy (2.13) identically. This set of solenoidal vectors must satisfy regularity conditions at the origin and homogeneous boundary conditions at the wall $r = 1$. It should be stressed that $r = 0$ is a regular singular point of the boundary value problem (2.12) when that problem is expressed in polar coordinates (there is no singularity in cartesian

coordinates). Therefore, in order to obtain analytic solutions in a neighbourhood of the origin, an analysis of the Taylor expansion of the vector fields will be needed. After obtaining the proper set of solenoidal functions, the operator (2.12) will be projected over another subspace of solenoidal vector fields whose regularity and boundary conditions will be studied in a moment. This method is a *Petrov-Galerkin* scheme, because the projection is carried out over a different set of functions from those used to expand the solution itself. The next section will deal with the regularity analysis of the approximating functions as well as symmetry and properties of the test–projection fields.

2.1 Linearized Navier-Stokes equation: regularity analysis

From now on, we consider perturbation fields of the form

$$\mathbf{u} = [v_r(r)\mathbf{e}_r + v_\theta(r)\mathbf{e}_\theta + v_z(r)\mathbf{e}_z]\mathrm{e}^{\mathrm{i}(kz+n\theta)}, \quad k \in \mathbb{R}, \quad n \in \mathbb{Z}. \tag{2.14}$$

With the previous functional structure, the explicit expressions of the linearized perturbation equation (2.12) become

$$\frac{1}{\mathrm{Re}}\left[D^2 v_r + \frac{1}{r}Dv_r - \left(\frac{n^2+1}{r^2} + k^2\right)v_r - \frac{2\mathrm{i}n}{r^2}v_\theta\right] - \mathrm{i}kw_B v_r = \lambda v_r, \tag{2.15}$$

$$\frac{1}{\mathrm{Re}}\left[D^2 v_\theta + \frac{1}{r}Dv_\theta - \left(\frac{n^2+1}{r^2} + k^2\right)v_\theta + \frac{2\mathrm{i}n}{r^2}v_r\right] - \mathrm{i}kw_B v_\theta = \lambda v_\theta, \tag{2.16}$$

$$\frac{1}{\mathrm{Re}}\left[D^2 v_z + \frac{1}{r}Dv_z - \left(\frac{n^2}{r^2} + k^2\right)v_z\right] - \mathrm{i}kw_B v_z - v_r Dw_B = \lambda v_z, \tag{2.17}$$

see (Meseguer, 1998), where $w_B(r)$ is the basic flow of (1.10) and $D = \mathrm{d}/\mathrm{d}r$. We do not include the pressure term $\nabla p'$ in this system because it will not affect our later computations. In fact, any gradient field will vanish when projecting over a solenoidal space. The perturbation field (v_r, v_θ, v_z) must satisfy the solenoidal condition (2.13), whose explicit expression is

$$Dv_r + \frac{1}{r}v_r + \frac{\mathrm{i}n}{r}v_\theta + \mathrm{i}kv_z = 0, \tag{2.18}$$

and no-slip boundary conditions at the wall,

$$v_r(1) = v_\theta(1) = v_z(1) = 0. \tag{2.19}$$

The regularity conditions will be determined by the boundedness of the solution (v_r, v_θ, v_z) over the centerline of the pipe ($r = 0$). As mentioned earlier, $r = 0$ is a regular singular point.

We consider the Taylor expansion of the fields (v_r, v_θ, v_z) as functions of r:

$$v_r(r) = a_0 + a_1 r + a_2 r^2 + a_3 r^3 + \cdots \tag{2.20}$$

$$v_\theta(r) = b_0 + b_1 r + b_2 r^2 + b_3 r^3 + \cdots \tag{2.21}$$

$$v_z(r) = c_0 + c_1 r + c_2 r^2 + c_3 r^3 + \cdots \tag{2.22}$$

Substitution of (2.20)–(2.22) in (2.15)–(2.17) gives the following expressions:

$$\begin{aligned} 2a_2 + 6a_3 r + \cdots + \frac{1}{r}[a_1 + 2a_2 r + 3a_3 r^2 + \cdots] \\ - \frac{n^2+1}{r^2}[a_0 + a_1 r + a_2 r^2 + \cdots] - k^2[a_0 + a_1 r + \cdots] \\ - \frac{2\mathrm{i}n}{r^2}[b_0 + b_1 r + b_2 r^2 + b_3 r^3 + \cdots] - \mathrm{i}k(1-r^2)[a_0 + a_1 r + \cdots]\mathrm{Re} \\ = \lambda[a_0 + a_1 r + a_2 r^2 \ + \cdots]\mathrm{Re} \end{aligned} \tag{2.23}$$

for the radial velocity,

$$\begin{aligned} 2b_2 + 6b_3 r + \cdots + \frac{1}{r}[b_1 + 2b_2 r + 3b_3 r^2 + \cdots] \\ - \frac{n^2+1}{r^2}[b_0 + b_1 r + b_2 r^2 + \cdots] - k^2[b_0 + b_1 r + \cdots] \\ + \frac{2\mathrm{i}n}{r^2}[a_0 + a_1 r + a_2 r^2 + a_3 r^3 + \cdots] - \mathrm{i}k(1-r^2)[b_0 + b_1 r + \cdots]\mathrm{Re} \\ = \lambda[b_0 + b_1 r + b_2 r^2 \ + \cdots]\mathrm{Re} \end{aligned} \tag{2.24}$$

for the azimuthal velocity, and

$$\begin{aligned} 2c_2 + 6c_3 r + \cdots + \frac{1}{r}[c_1 + 2c_2 r + 3c_3 r^2 + \cdots] \\ - \frac{n^2}{r^2}[c_0 + c_1 r + c_2 r^2 + \cdots] - k^2[c_0 + c_1 r + \cdots] \\ - \mathrm{i}k(1-r^2)[c_0 + c_1 r + \cdots]\mathrm{Re} - 2r[a_0 + a_1 r + a_2 r^2 + \cdots]\mathrm{Re} \\ = \lambda[c_0 + c_1 r + c_2 r^2 \ + \cdots]\mathrm{Re} \end{aligned} \tag{2.25}$$

for the axial velocity.

In the limit $r \to 0$, the left-hand sides of equations (2.23), (2.24) and (2.25) are bounded only if the following relations between the coefficients a_i, b_j, c_k are satisfied:

$$(n^2+1)a_0 + 2\mathrm{i}nb_0 = 0, \tag{2.26}$$

$$n^2 a_1 + 2\mathrm{i}nb_1 = 0, \tag{2.27}$$

$$2\mathrm{i}na_0 - (n^2+1)b_0 = 0, \tag{2.28}$$

$$2\mathrm{i}na_1 - n^2 b_1 = 0 \tag{2.29}$$

for the first coefficients of the radial and azimuthal components of the perturbation, and

$$n^2 c_0 = 0, \tag{2.30}$$

$$c_1(1-n^2) = 0 \tag{2.31}$$

for the first coefficients of the axial component. A straightforward analysis of the compatibility for the systems (2.27), (2.29), (2.26), (2.28), (2.30) and (2.31) leads to the restrictions on the coefficients listed in Table 1.

n	a_0	b_0	c_0	a_1	b_1	c_1
0	0	0	λ	μ	ν	0
± 1	λ	$\pm \mathrm{i}\lambda$	0	0	0	μ
± 2	0	0	0	λ	$\pm \mathrm{i}\lambda$	0
$\pm 3, \pm 4, \ldots$	0	0	0	0	0	0

Table 1: Table of the regularized 0th and 1st order coefficients of the perturbation field. The symbols λ, μ and ν stand for free parameters. The prescribed values are valid for any value of k.

n	a_0	b_0	c_0	a_1	b_1	c_1
0	0	0	μ	$-\mu \mathrm{i}k/2$	λ	0
± 1	λ	$\pm \mathrm{i}\lambda$	0	0	0	μ
± 2	0	0	0	λ	$\pm \mathrm{i}\lambda$	0
$\pm 3, \pm 4, \ldots$	0	0	0	0	0	0

Table 2: Table of the regularized 0th and 1st order coefficients of the perturbation field modified to satisfy the solenoidal condition (2.18). The symbols λ and μ stand for free parameters.

The solenoidal condition (2.18) may impose more restrictions on the previous coefficients. Substitution of the expansions (2.20)–(2.22) in (2.18) leads to the condition

$$a_1 + 2a_2 r + \cdots + \frac{1}{r}[a_0 + a_1 r + a_2 r^2 + \cdots] + \frac{\mathrm{i}n}{r}[b_0 + b_1 r + b_2 r^2 + \cdots] + \mathrm{i}k[c_0 + c_1 r + \cdots] = 0. \tag{2.32}$$

In order for (2.18) be satisfied in the limit $r \to 0$, the coefficients a_i, b_j and c_k must satisfy the following relations:

$$a_0 + \mathrm{i}nb_0 = 0, \tag{2.33}$$

$$2a_1 + \mathrm{i}nb_1 + \mathrm{i}kc_0 = 0. \tag{2.34}$$

The conditions (2.34) and (2.33) introduce only a minor change in a_1 for $n = 0$ (see Table 2).

2.2 Analyticity of vector fields in polar coordinates

So far we have derived some restrictions for the solenoidal perturbation fields. Boundedness of fields as well as the solenoidal condition at the origin have been imposed in order to have a better understanding of the local behaviour. Nevertheless, these conditions do not ensure that the functions are analytic in a neighbourhood of the origin. The restrictions obtained so far concern regularity of solutions of a system of differential equations, which only requires differentiability.

In order to have spectral accuracy in the numerical approximation of the eigenvalue problem, analyticity of the vector fields is required in the interval $[0, 1]$. Transformations to polar coordinates are singular at $r = 0$, making necessary a special treatment of our solution functions in a neighbourhood of the origin. At this point, we must think of a complex variable

problem instead of a real one. The domain of our problem is $\Omega = \{z \in \mathbb{C},\ |z| \leq 1\}$. The analyticity of the vector fields in the polar axis is ensured provided that the components satify the following property:

Theorem 2.1 (Priymak & Miyazaki) *Consider an analytic vector field* $\mathbf{u}(r,\theta) = \mathrm{e}^{\mathrm{i}n\theta}[v_r(r)\hat{\mathrm{e}}_r + v_\theta(r)\hat{\mathrm{e}}_\theta + v_z(r)\hat{\mathrm{e}}_z]$ $(n \in \mathbb{Z})$ *for* $r \leq \epsilon$ *for some* $\epsilon > 0$. *The radial, azimuthal and axial components of* $\mathbf{u}$ *must satisfy the following conditions :*

$$v_r = rf_E(r), \qquad v_\theta = rg_E(r) \quad (n = 0) \tag{2.35}$$

$$v_r = r^{|n|-1}f_E(r), \quad v_\theta = r^{|n|-1}g_E(r) \quad (n \neq 0) \tag{2.36}$$

for the radial and azimuthal components, and

$$v_z = r^{|n|}h_E(r) \quad (\forall n \in \mathbb{Z}) \tag{2.37}$$

for the axial component, where f_E, g_E *and* h_E *are functions which are analytic and even.*

From the coefficients listed in table 2, it can be demonstrated that our solenoidal solutions satisfy the conditions of theorem 2.1. In addition, a straightforward Frobenius method provides the right parity conditions required by this theorem. In fact, equations (2.15)–(2.17) are *Bessel*-type differential equations. Therefore, for n *even*, n^2 in (2.17) is also even, but n^2+1 in (2.15) and (2.16) is odd, v_z being an even function. By the same rule, v_r and v_θ are odd functions. The same reasoning can be applied for n *odd*. For a more detailed explanation of the symmetry and analyticity of polar vector fields see (Boyd, 1999), (Canuto *et al.*, 1988) or (Priymak & Miyazaki, 1998), for example.

2.3 Analytic solenoidal bases and Petrov-Galerkin projection

This section deals with the generation of solenoidal bases for our approximation of the vector field, which take the form

$$\mathbf{u} = \mathrm{e}^{\mathrm{i}(kz+n\theta)} \sum_{m=0}^{M} a_m^{(1)}\mathbf{v}_m^{(1)} + a_m^{(2)}\mathbf{v}_m^{(2)} \tag{2.38}$$

and satisfy the analyticity and parity conditions of last section. The fields $\mathbf{v}_m^{(1)}$ and $\mathbf{v}_m^{(2)}$ satisfy the zero-divergence condition

$$\nabla \cdot [\mathrm{e}^{\mathrm{i}(kz+n\theta)}\mathbf{v}_m^{(1,2)}] = 0. \tag{2.39}$$

Our main goal is to approximate solutions of the eigenvalue problem (2.15)–(2.17) by a spectral expansion (2.38). After substitution of the spectral expansion in the eigenvalue problem, the linearized operator is projected over another subspace of divergence-free fields (the dual or test space). Therefore, two different sets of vector fields are needed, one for the physical or trial space, and the other for the dual or test space, both solenoidal.

There are many different ways of obtaining divergence-free fields in polar coordinates, (see (Moser *et al.*, 1983) for example). We proceed in the same way as in appendix C of (Meseguer, 1998). The solenoidal condition (2.18) introduces a linear dependence between the components v_r, v_z and v_θ. Therefore, there are only two degrees of freedom. We will distinguish four different situations, streamwise dependent or independent and axisymmetric or non–axisymmetric fields:

- **Case I:** *Axisymmetric streamwise dependent* ($k \neq 0$, $n = 0$).

Regarding the explicit solenoidal condition (2.18) for $n = 0$,

$$\left(D + \frac{1}{r}\right) v_r + \mathrm{i}kv_z = 0, \tag{2.40}$$

we have a linear dependence between the components of the vector field. We make use of matrix notation in order to identify radial, azimuthal and axial components:

$$\begin{pmatrix} v_r \\ v_\theta \\ v_z \end{pmatrix} = v_r \mathbf{e}_r + v_\theta \mathbf{e}_\theta + v_z \mathbf{e}_z. \tag{2.41}$$

In this case, equation (2.40) introduces a dependence between radial and axial components, rendering the azimuthal one free. In other words, any element of this subspace can be expressed in the form

$$\begin{pmatrix} V_r \\ V_\theta \\ V_z \end{pmatrix} = \alpha \begin{pmatrix} 0 \\ v_\theta \\ 0 \end{pmatrix} + \beta \begin{pmatrix} -\mathrm{i}kv_r \\ 0 \\ D_+ v_r \end{pmatrix}, \tag{2.42}$$

where $D_+ = D + \frac{1}{r}$. Our aim is now to find suitable functions v_r and v_θ such that the conditions of theorem 2.1 as well as homogenous boundary conditions are satisfied. For the azimuthal component we consider

$$v_\theta(r) = r\mathrm{h}_m(r), \tag{2.43}$$

where

$$\mathrm{h}_m(r) = (1 - r^2)\mathrm{T}_{2m}(r) \tag{2.44}$$

In the definition of the function $\mathrm{h}_m(r)$, $\mathrm{T}_{2m}(r)$ stands for the Chebyshev polynomial of order $2m$. The factor $(1 - r^2)$ is added to make the vector field vanish over the wall. The factor r is necessary so that the analyticity conditions of theorem 2.1 are satisfied at the origin. Note that a factor $(1 - r)$ would provide the right boundary condition, but wrong parity for the theorem. We proceed in the same way for the radial component:

$$v_r(r) = r\mathrm{g}_m(r), \tag{2.45}$$

where

$$\mathrm{g}_m(r) = (1 - r^2)^2\mathrm{T}_{2m}(r). \tag{2.46}$$

In this case the binomial $(1 - r^2)$ is squared because the axial component also must vanish at $r = 1$. Again, a factor $(1 - r)^2$ would solve the boundary problem, but it would violate the parity imposed by theorem 2.1. The physical or trial basis is

$$\mathbf{v}_m^{(1)} = \begin{pmatrix} 0 \\ r\mathrm{h}_m(r) \\ 0 \end{pmatrix}, \quad \mathbf{v}_m^{(2)} = \begin{pmatrix} -\mathrm{i}kr\mathrm{g}_m(r) \\ 0 \\ D_+[r\mathrm{g}_m(r)] \end{pmatrix}. \tag{2.47}$$

We consider here the projection procedure in which the radial integration is involved. The radial hermitian product is defined by the volume integral

$$(\mathbf{a},\mathbf{b}) = \int_0^1 \mathbf{a}^* \cdot \mathbf{b}\; r\mathrm{d}r, \tag{2.48}$$

where $\mathbf{b}$ belongs to the physical or trial space and $\mathbf{a}$ is a solenoidal vector field belonging to the test or projection space. In order to take advantage of orthogonality properties of Chebyshev polynomials, the test functions are going to be built up suitably. In essence, the projection fields are going to have the same structure as the trial fields but the functions $\mathrm{h}_m(r)$ and $\mathrm{g}_m(r)$ will be modified by the Chebyshev weight $(1-r^2)^{-1/2}$. We make the following *ansatz*:

$$v_\theta(r) = r^{l_1}\tilde{\mathrm{h}}_m(r) = r^{l_1}\frac{\mathrm{h}_m(r)}{\sqrt{1-r^2}}, \tag{2.49}$$

$$v_r(r) = r^{l_2}\tilde{\mathrm{g}}_m(r) = r^{l_2}\frac{\mathrm{g}_m(r)}{\sqrt{1-r^2}}, \tag{2.50}$$

for the azimuthal and radial components, respectively. The exponents l_1 and l_2 are suitable integers such that there are no negative powers of r in the integrand of (2.48). In addition, because Chebyshev polynomials are orthogonal in the interval $[-1,1]$, we have to relate the integral (2.48) to a proper integral in which orthogonality can be applied. This is possible if the integrand $(\mathbf{a}^* \cdot \mathbf{b}) \quad r$ is an even function. In this case,

$$\int_0^1 \mathbf{a}^* \cdot \mathbf{b} \quad r\mathrm{d}r = \frac{1}{2}\int_{-1}^1 \mathbf{a}^* \cdot \mathbf{b} \quad r\mathrm{d}r \tag{2.51}$$

The evenness condition will determine finally the values of the exponents l_1 and l_2 in (2.49) and (2.50), respectively. In this case, $l_1 = 0$ and $l_2 = 2$ are the lowest powers which satisfy the previous conditions. To sum up, the dual or test basis is

$$\tilde{\mathbf{v}}_m^{(1)} = \frac{1}{\sqrt{1-r^2}}\begin{pmatrix} 0 \\ \mathrm{h}_m(r) \\ 0 \end{pmatrix}, \quad \tilde{\mathbf{v}}_m^{(2)} = \frac{1}{\sqrt{1-r^2}}\begin{pmatrix} \mathrm{i}kr^2\mathrm{g}_m(r) \\ 0 \\ D_+[r^2\mathrm{g}_m(r)] + r^3\mathrm{h}_m(r) \end{pmatrix}, \tag{2.52}$$

whose components have been already conjugated. The right-hand side integral in (2.51) can be computed exactly by Gauss-Chebyshev-Lobatto quadrature formulas. Again, the evenness of the integrand will be used in order to avoid unnecessary computations. We will only consider half a Gauss–Lobatto mesh. From this point of view, analyticity imposes some restrictions which can be used to optimize the computational cost.

The bases for the other three cases can be obtained after a little calculation considering the same criteria just explained.

- **Case II:** *Non-axysimmetric streamwise dependent* ($k \neq 0$, $n \neq 0$)

The physical basis is

$$\mathbf{v}_m^{(1)} = \begin{pmatrix} -\mathrm{i}nr^{|n|-1}\mathrm{g}_m(r) \\ D[r^{|n|}\mathrm{g}_m(r)] \\ 0 \end{pmatrix}, \quad \mathbf{v}_m^{(2)} = \begin{pmatrix} 0 \\ -\mathrm{i}kr^{|n|+1}\mathrm{h}_m(r) \\ \mathrm{i}nr^{|n|}\mathrm{h}_m(r) \end{pmatrix} \tag{2.53}$$

and the dual basis is

$$\tilde{\mathbf{v}}_m^{(1)} = \frac{1}{\sqrt{1-r^2}} \begin{pmatrix} \mathrm{i}nr\mathrm{g}_m(r) \\ D[r^2\mathrm{g}_m(r)] + r^3\mathrm{h}_m(r) \\ 0 \end{pmatrix}, \quad \tilde{\mathbf{v}}_m^{(2)} = \frac{1}{\sqrt{1-r^2}} \begin{pmatrix} 0 \\ -\mathrm{i}kr^3\mathrm{h}_m(r) \\ \mathrm{i}nr^2\mathrm{h}_m(r) \end{pmatrix} \tag{2.54}$$

for *n odd* or

$$\tilde{\mathbf{v}}_m^{(1)} = \frac{1}{\sqrt{1-r^2}} \begin{pmatrix} \mathrm{i}n\mathrm{g}_m(r) \\ D[r\mathrm{g}_m(r)] + r^2\mathrm{h}_m(r) \\ 0 \end{pmatrix}, \quad \tilde{\mathbf{v}}_m^{(2)} = \frac{1}{\sqrt{1-r^2}} \begin{pmatrix} 0 \\ -\mathrm{i}kr^2\mathrm{h}_m(r) \\ \mathrm{i}nr\mathrm{h}_m(r) \end{pmatrix} \tag{2.55}$$

for *n even*.

- **Case III:** *Axisymmetric streamwise independent* ($k = 0$, $n = 0$)

The physical basis is

$$\mathbf{v}_m^{(1)} = \begin{pmatrix} 0 \\ r\mathrm{h}_m(r) \\ 0 \end{pmatrix}, \quad \mathbf{v}_m^{(2)} = \begin{pmatrix} 0 \\ 0 \\ \mathrm{h}_m(r) \end{pmatrix} \tag{2.56}$$

and the dual basis is

$$\tilde{\mathbf{v}}_m^{(1)} = \frac{1}{\sqrt{1-r^2}} \begin{pmatrix} 0 \\ \mathrm{h}_m(r) \\ 0 \end{pmatrix}, \quad \tilde{\mathbf{v}}_m^{(2)} = \frac{1}{\sqrt{1-r^2}} \begin{pmatrix} 0 \\ 0 \\ r\mathrm{h}_m(r) \end{pmatrix} \tag{2.57}$$

- **Case IV:** *Non-axysimmetric streamwise independent* ($k = 0$, $n \neq 0$)

The physical basis is

$$\mathbf{v}_m^{(1)} = \begin{pmatrix} -\mathrm{i}nr^{|n|-1}\mathrm{g}_m(r) \\ D[r^{|n|}\mathrm{g}_m(r)]\mathrm{h}_m(r) \\ 0 \end{pmatrix}, \quad \mathbf{v}_m^{(2)} = \begin{pmatrix} 0 \\ 0 \\ r^{|n|}\mathrm{h}_m(r) \end{pmatrix} \tag{2.58}$$

and the dual basis is

$$\tilde{\mathbf{v}}_m^{(1)} = \frac{1}{\sqrt{1-r^2}} \begin{pmatrix} \mathrm{i}n\mathrm{g}_m(r) \\ D[r\mathrm{g}_m(r)] + r^2\mathrm{h}_m(r) \\ 0 \end{pmatrix}, \quad \tilde{\mathbf{v}}_m^{(2)} = \frac{1}{\sqrt{1-r^2}} \begin{pmatrix} 0 \\ 0 \\ r\mathrm{h}_m(r) \end{pmatrix} \tag{2.59}$$

for *n even*, and

$$\tilde{\mathbf{v}}_m^{(1)} = \frac{1}{\sqrt{1-r^2}} \begin{pmatrix} \mathrm{i}nr\mathrm{g}_m(r) \\ D[r^2\mathrm{g}_m(r)] + r^3\mathrm{h}_m(r) \\ 0 \end{pmatrix}, \quad \tilde{\mathbf{v}}_m^{(2)} = \frac{1}{\sqrt{1-r^2}} \begin{pmatrix} 0 \\ 0 \\ \mathrm{h}_m(r) \end{pmatrix} \tag{2.60}$$

for *n odd*.

The Petrov-Galerkin projection scheme is carried out by substituting the spectral approximation (2.38) in equations (2.15)–(2.17) and projecting over the dual space. This procedure leads to a discretized generalized eigenvalue problem

$$\lambda A(n,k)v = B_{\mathrm{Re}}(n,k)v, \tag{2.61}$$

where B_{Re} is a matrix which depends on Re number. In addition, the matrices A and B_{Re} depend on n and k, being decoupled for each pair of them. The explicit matrix elements of A are provided by the hermitian products

$$A_{ij} = (\tilde{\mathbf{v}}_i, \mathbf{v}_j), \quad B_{ij} = (\tilde{\mathbf{v}}_i, \mathcal{L}[\mathbf{v}_j]) \quad (0 \leq i, j \leq M), \tag{2.62}$$

where $\mathcal{L}$ stands for the linear operator

$$\mathcal{L}[\cdot] = \frac{1}{\mathrm{Re}}\Delta[\cdot] - \mathbf{v}_B \cdot \nabla[\cdot] - [\cdot] \cdot \nabla \mathbf{v}_B, \tag{2.63}$$

and where three hermitian product is the volume integral

$$(\tilde{\Psi}, \Phi) = \int_0^1 r\mathrm{d}r \int_0^{2\pi} \mathrm{d}\theta \int_0^{2\pi/k} \mathrm{d}z (\tilde{\Psi}^* \cdot \Phi). \tag{2.64}$$

We note here that the pressure term $\nabla p'$ should be formally included in the operator $\mathcal{L}$, but it is cancelled when projecting it over $\tilde{\Psi}$

$$(\tilde{\Psi}, \nabla p') = 0.$$

2.4 The linear initial value problem

In this section, we consider the linear initial value problem associated with the infinitesimal perturbations. We consider again the linearized equation (2.8) for the perturbation field

$$\partial_t \mathbf{u} = \frac{1}{\mathrm{Re}}\Delta \mathbf{u} - (\mathbf{v}_B \cdot \nabla)\mathbf{u} - (\mathbf{u} \cdot \nabla)\mathbf{v}_B, \tag{2.65}$$

where we have dropped the pressure term corresponding to the perturbation of the basic pressure field, because it will not affect our spectral approximation of the problem. Equation (2.65) can be expressed in a more compact form

$$\partial_t \mathbf{u} = \mathcal{L}_{\mathrm{Re}}[\mathbf{u}], \tag{2.66}$$

where $\mathcal{L}_{\mathrm{Re}}$ stands for the linear Laplacian-advective operator

$$\mathcal{L}_{\mathrm{Re}}[\cdot] = \frac{1}{\mathrm{Re}}\Delta[\cdot] - (\mathbf{v}_B \cdot \nabla)[\cdot] - ([\cdot] \cdot \nabla)\mathbf{v}_B, \tag{2.67}$$

which explicitly depends on Re. The next step is to transform (2.66) to a dynamical system of amplitudes which govern the temporal behaviour of the perturbation. It is this purpose that we use a Petrov-Galerkin projection scheme. The perturbation field will have the general structure

$$\mathbf{u}(r, \theta, z, t) = \sum_l \sum_n \sum_m a^{(1)}_{lmn}(t)\Phi^{(1)}_{lmn}(r, \theta, z) + a^{(2)}_{lmn}(t)\Phi^{(2)}_{lnm}(r, \theta, z), \tag{2.68}$$

where $\Phi^{(1,2)}_{lmn}$ are the basis of solenoidal vector fields described in section 2.3,

$$\Phi^{(1,2)}_{lnm}(r, \theta, z) = \mathrm{e}^{\mathrm{i}[l\kappa z + n\theta]}\mathbf{v}^{(1,2)}_m(r), \tag{2.69}$$

where $\mathbf{v}_m^{(1,2)}$ are prescribed in (2.47), (2.53), (2.56) and (2.58). These functions satisfy identically the zero-divergence condition

$$\nabla \cdot \Phi_{lnm}^{(1,2)} = 0 \tag{2.70}$$

in addition to regularity conditions over the axis and homogeneous boundary conditions over the wall. In order to project the equation (2.66), a dual basis of test vectors is going to be considered as was done in section 2.3. In this case, the dual basis is

$$\tilde{\Psi}_{lnm}^{(1,2)}(r,\theta,z) = \mathrm{e}^{\mathrm{i}[l\kappa z + n\theta]}\tilde{\mathbf{v}}_m^{(1,2)}(r), \tag{2.71}$$

where $\tilde{\mathbf{v}}_m^{(1,2)}$ are the vector fields prescribed in equations (2.52), (2.54), (2.55), (2.57), (2.59) or (2.60), depending on each particular case.

A (L,N,M)–order spectral approximation $\mathbf{u}$ for equation (2.66) is defined by

$$\mathbf{u}_{LNM}(r,\theta,z,t) = \sum_{l=-L}^{L}\sum_{n=-N}^{N}\sum_{m=-M}^{M} a_{lmn}^{(1)}(t)\Phi_{lmn}^{(1)}(r,\theta,z) + a_{lmn}^{(2)}(t)\Phi_{lmn}^{(2)}(r,\theta,z), \tag{2.72}$$

where L, N and M are the approximation orders of the axial, azimuthal and radial coordinates, respectively. The coefficients $a^{(1,2)}(t)$ govern the temporal behaviour of the perturbation. The Petrov-Galerkin scheme is formulated by introducing (2.72) into (2.66) and projecting over the set of dual vectors (2.71):

$$(\tilde{\Psi}_{lnm}^{(1,2)}, \partial_t \mathbf{u}_{LNM}) = (\tilde{\Psi}_{lnm}, \mathcal{L}_{\mathrm{Re}}[\mathbf{u}_{LNM}]), \quad (|l| \le L, \quad |n| \le N, \quad 0 \le m \le M). \tag{2.73}$$

The following orthogonality relations are useful in order to take advantage of azimuthal and axial symmetries:

$$\int_0^{2\pi} \mathrm{e}^{\mathrm{i}(n'-n)\theta}\mathrm{d}\theta = 2\pi\delta_{n'}^{n} \quad \text{and} \quad \int_0^{2\pi/\kappa} \mathrm{e}^{\mathrm{i}\kappa(l'-l)z}\mathrm{d}z = \frac{2\pi}{\kappa}\delta_{l'}^{l}, \tag{2.74}$$

where δ_j^i is the Kronecker symbol. In other words, the linear problem (2.66) is decoupled into each azimuthal and axial mode (n,l). Therefore, we have $(2L+1)\times(2N+1)$ independent linear systems of the form

$$\begin{bmatrix} (\tilde{\mathbf{v}}_m^{(1)}, \mathbf{v}_n^{(1)}) & (\tilde{\mathbf{v}}_m^{(1)}, \mathbf{v}_n^{(2)}) \\ (\tilde{\mathbf{v}}_m^{(2)}, \mathbf{v}_n^{(1)}) & (\tilde{\mathbf{v}}_m^{(2)}, \mathbf{v}_n^{(2)}) \end{bmatrix} \begin{bmatrix} \dot{a}_n^{(1)} \\ \dot{a}_n^{(2)} \end{bmatrix} = \begin{bmatrix} (\tilde{\mathbf{v}}_m^{(1)}, \mathcal{L}_{\mathrm{Re}}[\mathbf{v}_n^{(1)}]) & (\tilde{\mathbf{v}}_m^{(1)}, \mathcal{L}_{\mathrm{Re}}[\mathbf{v}_n^{(2)}]) \\ (\tilde{\mathbf{v}}_m^{(2)}, \mathcal{L}_{\mathrm{Re}}[\mathbf{v}_n^{(1)}]) & (\tilde{\mathbf{v}}_m^{(2)}, \mathcal{L}_{\mathrm{Re}}[\mathbf{v}_n^{(2)}]) \end{bmatrix} \begin{bmatrix} a_n^{(1)} \\ a_n^{(2)} \end{bmatrix}, \tag{2.75}$$

as a Mth-order discretization of (2.66) whose dimension is $2(M+1)$. Symbolically, (2.75) can be re-written as

$$A\dot{a} = B_{\mathrm{Re}}a, \tag{2.76}$$

where A and B_{Re} are just the matrices which appeared in the generalized eigenvalue problem (2.61). In order to simplify the notation, we are going to omit the l and n indexes. We are going to develop our formulation for one axial-azimuthal mode (l,n). It must be understood that this formulation can be extended in the same way to any other axial or azimuthal components.

2.5 Energy norm for the perturbation fields

Any solenoidal perturbation can be expressed as a linear combination of the functions $\mathbf{v}_m^{(1,2)}$,

$$\mathbf{u} = [a_0^{(1)}\, a_1^{(1)}\, \cdots\, a_M^{(1)}\, ;\, a_0^{(2)}\, a_1^{(2)}\, \cdots\, a_M^{(2)}]^T = \sum_{m=0}^{M} a_m^{(1)}\mathbf{v}_m^{(1)} + a_m^{(2)}\mathbf{v}_m^{(2)}, \tag{2.77}$$

and we can view the coefficients involved as a vectorial representation of $\mathbf{u}$. In this representation, the 2-norm of $\mathbf{u}$ is

$$||\mathbf{u}||_2^2 = \sum_{m=0}^{M} |a_m^{(1)}|^2 + |a_m^{(2)}|^2. \tag{2.78}$$

When considering the *energy density of a perturbation*, we must calculate the quantity

$$\mathcal{E} = \frac{1}{2}(\mathbf{u}^*, \mathbf{u}), \tag{2.79}$$

where $(\cdot,\cdot)$ is the standard volume inner product defined previously. The basis $\mathbf{v}_m^{(1,2)}$ is *non-orthonormal*, i.e. $(\mathbf{v}_i^{(\alpha)*}, \mathbf{v}_j^{(\beta)}) \neq \delta_{ij}\delta^{\alpha\beta}$. Therefore, $||\mathbf{u}||_2^2 \neq (\mathbf{u}^*, \mathbf{u})$. In other words, we need the matrix of inner products $\mathcal{M}_{ij} = (\mathbf{v}_i^{(1,2)*}, \mathbf{v}_j^{(1,2)})$ for the energy norm of the perturbation. This matrix is

$$\mathcal{M}_{ij} = \begin{bmatrix} (\mathbf{v}_i^{(1)*}, \mathbf{v}_j^{(1)}) & (\mathbf{v}_i^{(1)*}, \mathbf{v}_j^{(2)}) \\ (\mathbf{v}_i^{(2)*}, \mathbf{v}_j^{(1)}) & (\mathbf{v}_i^{(2)*}, \mathbf{v}_j^{(2)}) \end{bmatrix}, \tag{2.80}$$

which would be the same as A in (2.76) if the projection were carried out through a Galerkin scheme. In this case, the functions $\mathbf{v}$ and $\tilde{\mathbf{v}}$ are not the same. To sum it up, the energy of the perturbation $\mathbf{u}$ is obtained via the weighted scalar product

$$\mathcal{E} = \frac{1}{2}[a_i^{(1)*}\, ;\, a_i^{(2)*}]\mathcal{M}_{ij} \begin{bmatrix} a_j^{(1)} \\ a_j^{(2)} \end{bmatrix}. \tag{2.81}$$

The matrix $\mathcal{M}$ is positive definite, so it can be factorized as $\mathcal{M} = \mathcal{F}^H\mathcal{F}$. This factorization can be obtained numerically using the QR algorithm (Trefethen & Bau, 1997). This decomposition will be used in a moment.

2.6 Eigenvalue decomposition

Provided that A is non-singular, the linear system (2.76) can be expressed as

$$\dot{a} = Ca, \tag{2.82}$$

where $C = A^{-1}B_{\mathrm{Re}}$. Consider the eigen subspace of the operator C

$$\mathcal{S}_M(C) = \mathrm{span}\{\mathbf{q}_1, \mathbf{q}_2, \ldots, \mathbf{q}_{2M+2}\}$$

spanned by the $2M+2$ eigenvectors of C. The system (2.82) can be expressed in its canonical form

$$\dot{\boldsymbol{\kappa}} = \Lambda\boldsymbol{\kappa}, \tag{2.83}$$

where

$$\boldsymbol{\kappa} = [\kappa_1,\, \kappa_2,\, \ldots\, , \kappa_{2M+2}]^T_{\mathcal{S}_M} \tag{2.84}$$

is the representation of the state vector in the eigenbasis $\mathcal{S}_M$ and Λ is the diagonal matrix of eigenvalues of C

$$\Lambda = \begin{bmatrix} \lambda_1 & 0 & \cdots & 0 \\ 0 & \lambda_2 & \cdots & 0 \\ \vdots & \vdots & \cdots & 0 \\ 0 & 0 & \cdots & \lambda_{2M+2} \end{bmatrix}. \tag{2.85}$$

The solution of the initial value problem (2.83) is

$$\boldsymbol{\kappa}(t) = \mathrm{e}^{\Lambda t}\boldsymbol{\kappa}(0). \tag{2.86}$$

An straightforward algebraic calculation provides the expression for the energy density associated with the state vector $\boldsymbol{\kappa}$

$$\mathcal{E} = \frac{1}{2}\,[\boldsymbol{\kappa}^H]\,[\mathcal{V}^H\mathcal{M}\mathcal{V}]\,[\boldsymbol{\kappa}] = \frac{1}{2}(\boldsymbol{\kappa},\boldsymbol{\kappa})_{\mathcal{M}}, \tag{2.87}$$

where $\mathcal{V}$ is the matrix of column eigenvectors $\mathbf{q}_i$ and $(\cdot,\cdot)_{\mathcal{M}}$ stands for the $\mathcal{V}^H\mathcal{M}\mathcal{V}$-weighted scalar product. Since the matrix $\mathcal{V}^H\mathcal{M}\mathcal{V}$ is positive definite, it admits a Cholesky decomposition

$$\mathcal{V}^H\mathcal{M}\mathcal{V} = \mathcal{F}^H\mathcal{F}, \tag{2.88}$$

which will be used in section §4. This decomposition is useful for the calculation of energy norms via computation of 2-norms. The relations between them are as follows:

$$||\mathcal{F}\boldsymbol{\kappa}||_2^2 = (\mathcal{F}\kappa,\mathcal{F}\kappa)_2 = (\kappa,\kappa)_{\mathcal{M}} = ||\boldsymbol{\kappa}||_{\mathcal{E}}^2, \tag{2.89}$$

where $||\cdot||_{\mathcal{E}}$ is the *energy norm* and $||\cdot||_2$ is the standard *2-norm*.

3 Linear stability: numerical results

For the linear stability analysis, we have solved the eigenvalue problem (2.61) for different values of n and k by the MATLAB code listed in Appendix A. The convergence and reliability of the code have been checked. For this purpose, some of the results reported here have been compared with previous works. For example, in Table 3, the convergence of the rightmost eigenvalue of (2.61) is reported for Re = 9600, a case treated in (Leonard & Wray, 1982), (Priymak & Miyazaki, 1998) and other former works:

- (Salwen *et al.*, 1980): $\lambda_1 = -0.02317 + 0.95048\,\mathrm{i}$
- (Leonard & Wray, 1982): $\lambda_1 = -0.023170795764 + 0.950481396668\,\mathrm{i}$
- (Priymak & Miyazaki, 1998): $\lambda_1 = -0.0231707957650042152055 + 0.9504813966699031794843\,\mathrm{i}$.

M	*size*	λ_1				CPU-time (s.)
20	42×42	−0.0229	+	0.950	i	0.2
30	62×62	−0.0231707	+	0.9504813	i	0.5
40	82×82	−0.02317079576	+	0.950481396669	i	0.9
50	102×102	−0.023170795764	+	0.950481396670	i	1.7

Table 3: Convergence test for Re = 9600, $k = 1$, $n = 1$, following (Priymak & Miyazaki, 1998) and (Leonard & Wray, 1982). M is the number of Chebyshev polynomials used in the spectral approximation, *size* is the dimension of the discretization matrix and λ_1 stands for the rightmost eigenvalue. CPU-time is the elapsed computation time on an Intel Celeron 300MHz processor. The reported figures are those which are apparently converged at M=60.

The last result was obtained using quadruple precision. For Re = 3000, the spectra for different values of k and n have been computed in order to make comparisons with a first comprehensive stability analysis carried out in (Schmid & Henningson, 1994). Our code provided spectral accuracy in all the computed cases. In Tables 4 and 5, the 40 rightmost eigenvalues have been listed for $k = 1$ and $k = 0, 1, 2, 3$.

The same computation has been done for streamwise-independent perturbations ($k = 0$) and for different values of the azimuthal mode n (see Table 6). As far as we know, numerical tables of streamwise-independent modes have not been reported previously. Mathematically, the case $k = 0$ must get a special treatment. In fact, the limit $k \to 0$ does not coincide with this case. In our formulation, this phenomenon can be understood looking at the boundary conditions which must be satisfied by the radial velocity over the wall. For $k \neq 0$, the radial velocity, as well as its first derivative, must vanish over the wall. For $k = 0$ the boundary conditions change abruptly. The solenoidal perturbation vector fields defined in (2.10) are invariant under spiral transformations of the form

$$\frac{\mathrm{d}z}{\mathrm{d}\theta} = -\frac{n}{k}. \tag{3.1}$$

Making use of the *spiral* coordinate $\zeta = n\theta + kz$, the solenoidal condition

$$\nabla \cdot \mathbf{v} = \frac{1}{r}\partial_r(rv_r) + \frac{1}{r}\partial_\theta v_\theta + \partial_z v_z = 0$$

can be expressed in this new variable as

$$\frac{1}{r}\partial_r(rv_r) + \partial_\zeta[\frac{n}{r}v_\theta + rkv_z] = 0, \tag{3.2}$$

where we have used the chain rules

$$\partial_\theta = (\partial_\theta\zeta)\partial_\zeta = n\partial_\zeta, \quad \partial_z = (\partial_z\zeta)\partial_\zeta = k\partial_\zeta.$$

Equation (3.2) can be expressed as

$$\partial_r(rv_r) + \partial_\zeta[nv_\theta + rkv_z] = 0, \tag{3.3}$$

which implies the existence of a first integral $\chi(r, \theta)$ of the perturbed field satisfiying

$$\partial_\zeta\chi = -rv_r, \tag{3.4}$$

$$\partial_r\chi = nv_\theta + rkv_z. \tag{3.5}$$

$n=0$				$n=1$			
−0.0519731112828	+	0.9483602220505	i	−0.041275644693	+	0.91146556762	i
−0.0519731232053	+	0.948360198487	i	−0.0616190180049	+	0.370935092697	i
−0.103612364039	+	0.896719200867	i	−0.088346025188	+	0.958205542989	i
−0.103612889227	+	0.8967204441	i	−0.0888701566	+	0.8547888174	i
−0.112217160388	+	0.4123963342099	i	−0.1168771535871	+	0.216803862997	i
−0.121310028246	+	0.2184358147279	i	−0.137490337	+	0.7996994696	i
−0.155220165293	+	0.8450717997117	i	−0.14434614486	+	0.91003730954	i
−0.155252667198	+	0.845080668126	i	−0.1864329862	+	0.7453043578	i
−0.2004630477669	+	0.3762423600255	i	−0.195839466	+	0.5493115826	i
−0.20647681141	+	0.79378412983	i	−0.198646109	+	0.8607494634	i
−0.20689284901	+	0.79344079903	i	−0.20495551139	+	0.37643141466	i
−0.2274656214	+	0.62629699816	i	−0.234333468	+	0.693462324	i
−0.257315715842	+	0.502037310431	i	−0.2518090868	+	0.5026425132	i
−0.25850846682	+	0.74175750308	i	−0.2521234956	+	0.8108448759	i
−0.25888061551	+	0.7470464722	i	−0.270458581649	+	0.3251302632238	i
−0.2975265027697	+	0.3473922918486	i	−0.2896472	+	0.65506433	i
−0.30105176512	+	0.610862593968	i	−0.3051265039	+	0.760702408	i
−0.30816630839445	+	0.6926062097	i	−0.30901045	+	0.60793447	i
−0.3243180595	+	0.7103043057	i	−0.34479048	+	0.587438025	i
−0.3705329662	+	0.6745795964	i	−0.3591401466	+	0.711236702	i
−0.381468165	+	0.6004524818	i	−0.365684003	+	0.660391529	i
−0.406650704	+	0.6823493566	i	−0.414686969	+	0.675874007	i
−0.4531867948	+	0.6728830197	i	−0.45142803	+	0.673368207	i
−0.496799418	+	0.67362375113	i	−0.497340377	+	0.671987037	i
−0.5422117348	+	0.6715149511	i	−0.5416003042	+	0.671459572	i
−0.58888608168	+	0.67172366336	i	−0.588958474	+	0.6707809915	i
−0.6369764697	+	0.67047421997	i	−0.6363554653	+	0.6703507747	i
−0.6864666756	+	0.67081597825	i	−0.6866042283	+	0.6699895489	i
−0.73763594554	+	0.66968289478	i	−0.7369640316	+	0.6695424132	i
−0.78999989327	+	0.670159603825	i	−0.7902088929	+	0.6694100369	i
−0.84431671482	+	0.66907755092	i	−0.8436119241	+	0.6689183737	i
−0.89961222728	+	0.66964463547	i	−0.8998742853	+	0.668973590013	i
−0.95712046594	+	0.6686110213	i	−0.9564003206	+	0.6684327237	i
−1.01539931983	+	0.66923128608	i	−1.01569748252	+	0.6686366096	i
−1.07612880212	+	0.66824851712	i	−1.07540622898	+	0.6680540404	i
−1.13743683309	+	0.66889435007	i	−1.137757699918	+	0.6683699588	i
−1.20140723325	+	0.66796443547	i	−1.2006907478	+	0.6677582895	i
−1.26578430228	+	0.66861621486	i	−1.2661180938	+	0.6681542463	i
−1.333008454262	+	0.667739900923	i	−1.3323030622	+	0.6675268175	i
−1.40048869474	+	0.66838419969	i	−1.40082868902	+	0.66797648159	i
−1.47097499114	+	0.66756093672	i	−1.47028318091	+	0.6673451475	i

Table 4: First 40 eigenvalues for Re = 3000, $k = 1$ and $n = 0, 1$, for comparison with (Schmid & Henningson, 1994). The figures reported are those that are apparently converged at $M = 54$ (a matrix of dimension approximately 108).

$n=2$				$n=3$			
-0.060285689559	$+$	0.88829765875	i	-0.08325397694	$+$	0.86436392104	i
-0.08789898037	$+$	0.352554927087	i	-0.105708407362	$+$	0.346401953386	i
-0.1088383407	$+$	0.8328933609	i	-0.116877921343	$+$	0.2149198697617	i
-0.112001616152	$+$	0.939497219531	i	-0.1323924331	$+$	0.8097468023	i
-0.1155143802215	$+$	0.215491816529	i	-0.136035459528	$+$	0.91671917468	i
-0.15810861	$+$	0.778584987	i	-0.182036372	$+$	0.7558793156	i
-0.167294045951	$+$	0.8906185726	i	-0.190639836903	$+$	0.8674136555	i
-0.20759146658	$+$	0.725077139	i	-0.2127794121	$+$	0.37123649827	i
-0.20931432998	$+$	0.37502653759	i	-0.23181786	$+$	0.70300722	i
-0.2214747313	$+$	0.8409753749	i	-0.244111241	$+$	0.551731632	i
-0.2282286376	$+$	0.5516823128	i	-0.2444955726	$+$	0.8175699979	i
-0.2498030523	$+$	0.5008719091	i	-0.251142783	$+$	0.499292178	i
-0.25796791	$+$	0.67522075	i	-0.2619068832	$+$	0.36144947997	i
-0.26313897737	$+$	0.34209716626	i	-0.28515317	$+$	0.655473	i
-0.2750370177	$+$	0.7908951089	i	-0.297844937	$+$	0.7674455592	i
-0.30889763	$+$	0.602773208	i	-0.307365548	$+$	0.59782813	i
-0.328199033	$+$	0.740925499	i	-0.34688562	$+$	0.62370102	i
-0.3321112	$+$	0.64008734	i	-0.35098742198	$+$	0.71809663	i
-0.34301682	$+$	0.61416043	i	-0.37620428	$+$	0.652416	i
-0.38299776	$+$	0.69296469	i	-0.41103456	$+$	0.677885117	i
-0.405976204	$+$	0.6664413	i	-0.449261963	$+$	0.668061	i
-0.453715394	$+$	0.67313573	i	-0.49600428	$+$	0.67047667	i
-0.494871994	$+$	0.670736754	i	-0.53862783	$+$	0.66818288	i
-0.541993243	$+$	0.670827765	i	-0.587534483	$+$	0.66941016	i
-0.586958536	$+$	0.669664695	i	-0.63326489	$+$	0.6673481726	i
-0.636547104	$+$	0.66998293547	i	-0.6848609	$+$	0.66893828	i
-0.68458947988	$+$	0.668767909	i	-0.7338322	$+$	0.66667637	i
-0.737028556	$+$	0.6694480681	i	-0.78816043	$+$	0.668645268	i
-0.78821114	$+$	0.668079502	i	-0.84049089	$+$	0.66618389	i
-0.843523627	$+$	0.6690644336	i	-0.897552143	$+$	0.668440187	i
-0.8979475001	$+$	0.667556087	i	-0.953322785	$+$	0.66583465	i
-0.956138941	$+$	0.6687743348	i	-1.013133742	$+$	0.668283474	i
-1.013877224	$+$	0.6671621441	i	-1.07238926	$+$	0.66559598	i
-1.074964494	$+$	0.6685446315	i	-1.13498331	$+$	0.66815399	i
-1.136061803	$+$	0.666868996	i	-1.19774082	$+$	0.66544103	i
-1.2000720529	$+$	0.668355358	i	-1.26316193	$+$	0.668040708	i
-1.264551366	$+$	0.66665349	i	-1.32942013	$+$	0.6653483	i
-1.3315179092	$+$	0.6681945884	i	-1.397716901	$+$	0.6679382	i
-1.399387494	$+$	0.6664971767	i	-1.46746351	$+$	0.66530119	i
-1.46934599514	$+$	0.6680551476	i	-1.538684797	$+$	0.66784398	i
-1.5406049725	$+$	0.666385603	i	-1.61190195	$+$	0.66528662	i

Table 5: Same as Table 4, but for $n = 2, 3$.

$n=0$	$n=1$	$n=2$	$n=3$
-0.0019277286542	-0.00489399021	-0.0087915387	-0.0135688219
-0.004893990214	-0.0087915388	-0.01356882195	-0.01919431362
-0.0101570874478	-0.0164061521	-0.0236166663	-0.03175919084
-0.01640615210723	-0.0236166663	-0.03175919085	-0.040809265355
-0.0249623355969	-0.03449981796	-0.04500690295	-0.0564651499
-0.034499817965	-0.045006902955	-0.05646514994	-0.06885660345
-0.0463467614754	-0.059173588937	-0.0729733963	-0.087733618
-0.0591735889378	-0.072973396381	-0.08773361808	-0.103440753288
-0.07431076787255	-0.090427218091	-0.1075183721	-0.1255751331
-0.0904272180909	-0.107518372097	-0.12557513314	-0.14458704546
-0.1088544509774	-0.128260635034	-0.1486425215	-0.1699932252
-0.1282606350342	-0.148642521512	-0.16999322529	-0.19230443298
-0.14997784283936	-0.17267381366	-0.19634611723	-0.2209893628
-0.1726738136706	-0.196346117238	-0.22098936279	-0.24659679175
-0.1976809565519	-0.22366674254	-0.25062928459	-0.278564248
-0.2236667425409	-0.250629284603	-0.278564248292	-0.30746603558
-0.2519637982613	-0.281239415979	-0.31149208784	-0.342718253
-0.28123941597896	-0.311492087829	-0.342718253295	-0.37491320196
-0.31282637115853	-0.345391830923	-0.3789345626	-0.41345158958
-0.3453918309236	-0.378934562605	-0.41345158953	-0.4489388946
-0.3802686770332	-0.416123985604	-0.45295673	-0.4907643848
-0.416123985604594	-0.452956730057	-0.49076438495	-0.5295434847
-0.4542907169513	-0.49343587894	-0.5335586033	-0.5746567206
-0.4934358789401	-0.533558603342	-0.57465672065	-0.61672721098
-0.53489249158	-0.57732751024	-0.6207401910159	-0.66512865
-0.5773275102394	-0.620740191	-0.665128650033	-0.71049023265
-0.6220740013539	-0.66779887904	-0.7145014987	-0.7621802093
-0.6677988790445	-0.714501498775	-0.76218020947	-0.8108326594
-0.7158352465659	-0.76484998504	-0.8148425305	-0.865811424
-0.7648499850421	-0.81484253064	-0.865811424448	-0.91775456872
-0.8161762274193	-0.86848082801	-0.92176328942	-0.976022313
-0.8684808280122	-0.921763289419	-0.97602231319	-1.03125601664
-0.9230969440588	-0.97869140779	-1.0352637772	-1.092812888
-0.978691407795	-1.035263777163	-1.09281288908	-1.1513370445
-1.0365973965894	-1.095481724277	-1.15534399534	-1.216183162
-1.095481724277	-1.155343995387	-1.21618316211	-1.2779976834
-1.1566775850891	-1.2188517773695	-1.2820039452	-1.3461331398
-1.21885177737	-1.282003945236	-1.34613313981	-1.41123795719
-1.2833375096168	-1.348801567	-1.41524362762	-1.482662828
-1.348801567007	-1.41524362758	-1.48266282802	-1.55105788401
-1.4165771702174	-1.48533109313	-1.55506304307	-1.625772231

Table 6: Same as Tables 4, 5 but for $k=0$, $n=0,1,2,3$.

The fluid particles are constrained to move over $\chi = const.$ surfaces. In other words, the function χ plays the role of a stream function which is tangent to the perturbation vector field $\mathbf{u}$. From equation (3.5) we can obtain χ for the different four cases described in §2.3. The physical vector field is a real object obtained when solving the eigenvalue problem for the conjugated modes $n \to -n$ and $k \to -k$:

$$\mathbf{u} = 2\Re\{\mathrm{e}^{\mathrm{i}(kz+n\theta)} \sum_{m=0}^{M} a_m^{(1)}\mathbf{v}_m^{(1)} + a_m^{(2)}\mathbf{v}_m^{(2)}\} \tag{3.6}$$

Again we provide here the explicit expressions of χ for each case:

- **Case I:** $k \neq 0$, $n = 0$

From expressions (2.47) and equation (3.5) we obtain

$$\partial_r\chi = rkv_z = 2k\Re\{\mathrm{e}^{\mathrm{i}(kz+n\theta)} \sum_{m=0}^{M} r[\partial_r(r\mathrm{g}_m) + \mathrm{g}_m]a_m^{(2)}\}, \tag{3.7}$$

and therefore

$$\chi = 2k\Re\{\mathrm{e}^{\mathrm{i}(kz+n\theta)} \sum_{m=0}^{M} a_m^{(2)}[\int r\partial_r(r\mathrm{g}_m)\mathrm{d}r + \int r\mathrm{g}_m]\mathrm{d}r\}. \tag{3.8}$$

Integrating the first integral by parts, we obtain

$$\chi = 2kr^2\Re\{\mathrm{e}^{\mathrm{i}(kz+n\theta)} \sum_{m=0}^{M} a_m^{(2)}\mathrm{g}_m(r)\} + \mathrm{C}, \tag{3.9}$$

where C is an arbitrary constant of integration.

- **Case II:** $k \neq 0$, $n \neq 0$

From expressions (2.53) and equation (3.5) we obtain

$$\partial_r\chi = nv_\theta + rkv_z = 2\Re\{\mathrm{e}^{\mathrm{i}(kz+n\theta)} \sum_{m=0}^{M} na_m^{(1)}\partial_r(r^{|n|}\mathrm{g}_m) - a_m^{(2)}nkr^{|n|+1}\mathrm{h}_m + a_m^{(2)}rknr^{|n|}\mathrm{h}_m\}. \tag{3.10}$$

Straightforward integration of this equation leads to

$$\chi = 2nr^{|n|}\Re\{\mathrm{e}^{\mathrm{i}(kz+n\theta)} \sum_{m=0}^{M} a_m^{(1)}\mathrm{g}_m(r)\} + \mathrm{C}. \tag{3.11}$$

- **Case III:** $k = 0$, $n = 0$

In this case, equation (3.5) leads to

$$\partial_r\chi = 0, \tag{3.12}$$

and

$$\chi = \mathrm{C}, \tag{3.13}$$

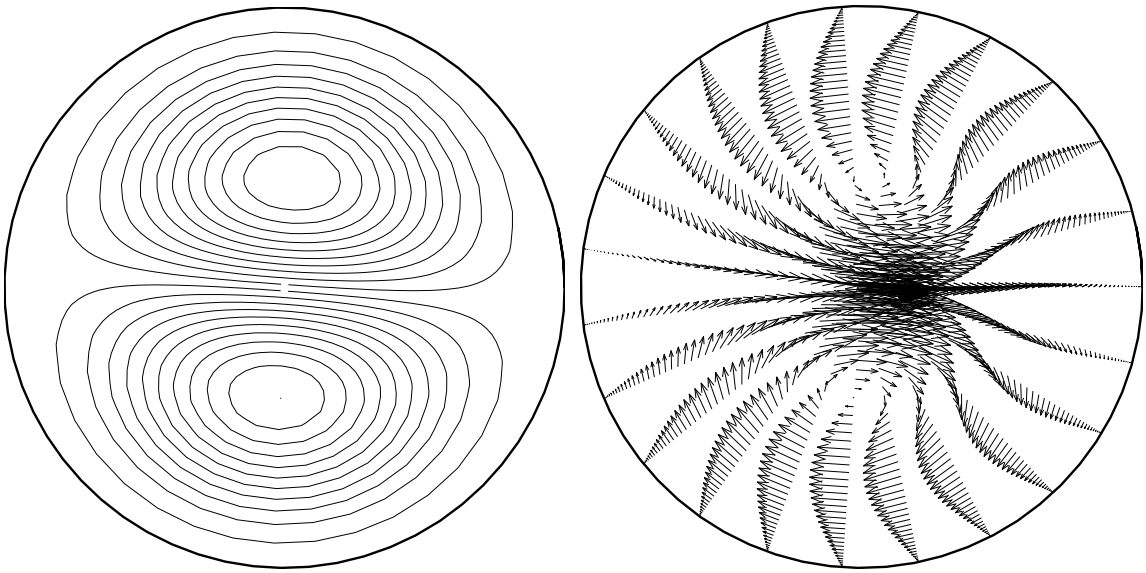

Figure 2: Constant-z cross sections of streamwise independent stream function and vector field corresponding to the $n = 1$, $k = 0$ eigenvalue $\lambda_2 = -0.0087915388$ for $\mathrm{Re} = 3000$.

- **Case IV:** $k = 0$, $n \neq 0$

For this case, expressions (2.58) lead to

$$\chi = 2nr^{|n|}\Re\{\mathrm{e}^{\mathrm{i}(kz+n\theta)} \sum_{m=0}^{M} a_m^{(1)} \mathrm{g}_m(r)\} + \mathrm{C}. \tag{3.14}$$

From the previous expressions, we have computed the *eigen*-stream functions and *eigen*-vector fields or eigenmodes associated with the least stable eigenvalues of the spectra of the operator. For example, in figure 4, the least stable eigenmode for $k = 1$, $n = 1$ has been plotted for $\mathrm{Re} = 3000$. The eigenmodes $k = 1$, $n = 2, 3$ have been plotted in figures 6 and 7. In figure 5 we have plotted the three dimensional invariant surfaces for $n = 3$ mode. Because these modes are of *center* type, the dynamics is localized around the axis of the cylinder. In order to have a better understanding of the structure of *wall* and *mean* modes, we have represented them in figures 8 and 9, respectively. We can observe that the dynamics of wall modes is mainly concentrated near the wall whether mean modes dynamics is localized in the mean radius of the pipe.

We have also computed the leading eigenvalues of the linear operator for different values of the axial wavenumber k (in the range $k \in [0, 1]$) and for different values of n, as done in (Trefethen *et al.*, 1999). A remarkable fact is that the parametric evolution of these eigenvalues is not continuous in the limit $k \to 0$, as can be observed in figure 10 for the axisymmetric case $n = 0$. Note that the curves exhibit a discontinuity as they approach the real axis over the complex plane. This feature was not reported in (Trefethen *et al.*, 1999). In these computations, the number of modes was $M = 50$.

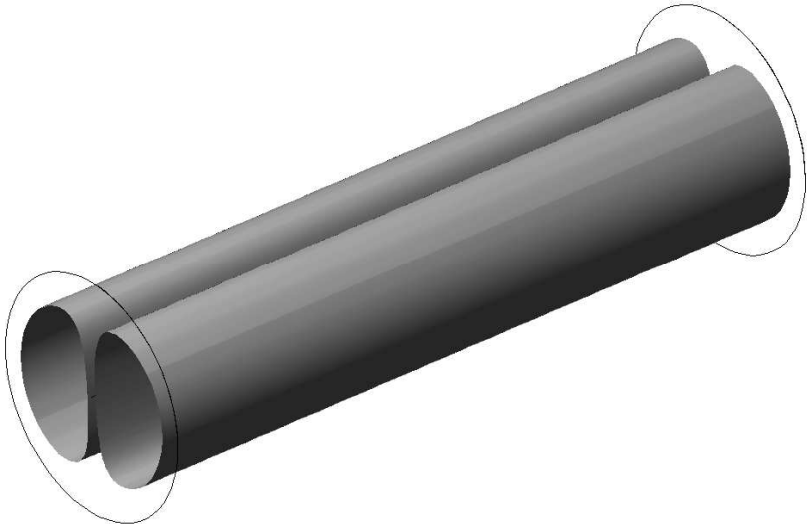

Figure 3: 3D structure of stream function χ corresponding to the $n = 1$, $k = 0$ streamwise mode $\lambda_2 = -0.0087915388$ for $\mathrm{Re} = 3000$.

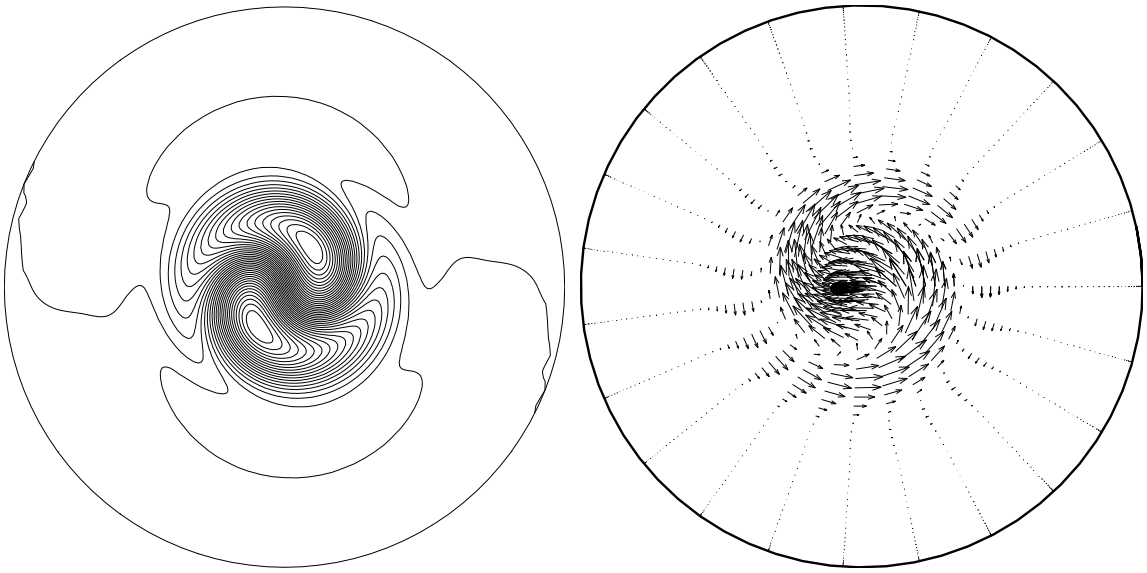

Figure 4: Constant-z cross sections of center-mode stream function and vector field corresponding to the $n = 1$, $k = 1$ least stable eigenvalue $\lambda_1 = -0.041275644693 + 0.91146556762\mathrm{i}$ for $\mathrm{Re} = 3000$.

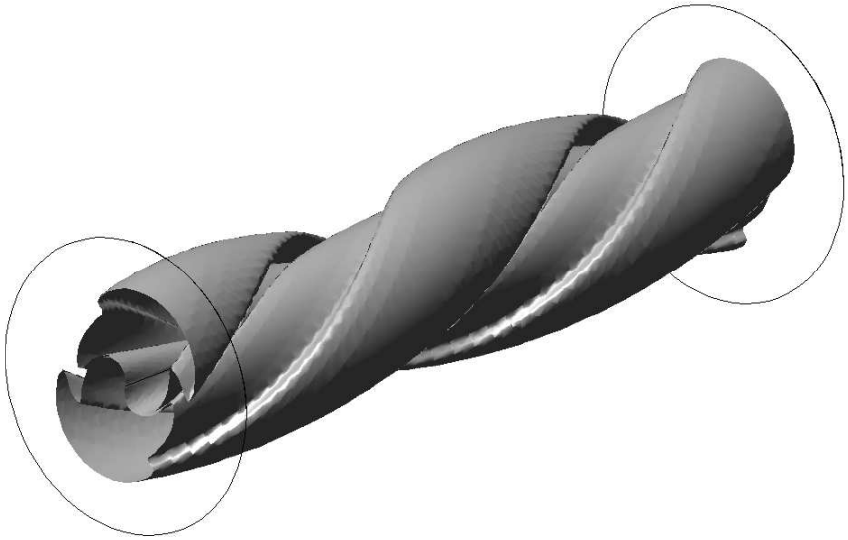

Figure 5: 3D structure of stream function χ corresponding to the $n = 1$, $k = 1$ least stable eigenvalue $\lambda_1 = -0.041275644693 + 0.91146556762\mathrm{i}$ for $\mathrm{Re} = 3000$.

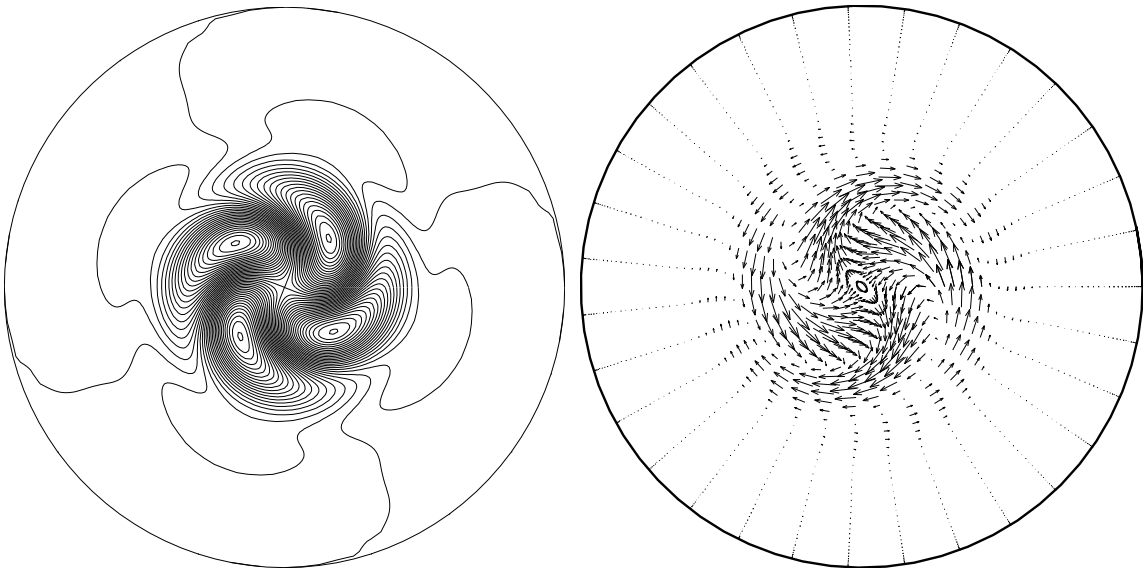

Figure 6: Constant-z cross sections of center-mode stream function and vector field corresponding to the $n = 2$, $k = 1$ least stable eigenvalue $\lambda_1 = -0.060285689559 + 0.88829765875\mathrm{i}$ for $\mathrm{Re} = 3000$.

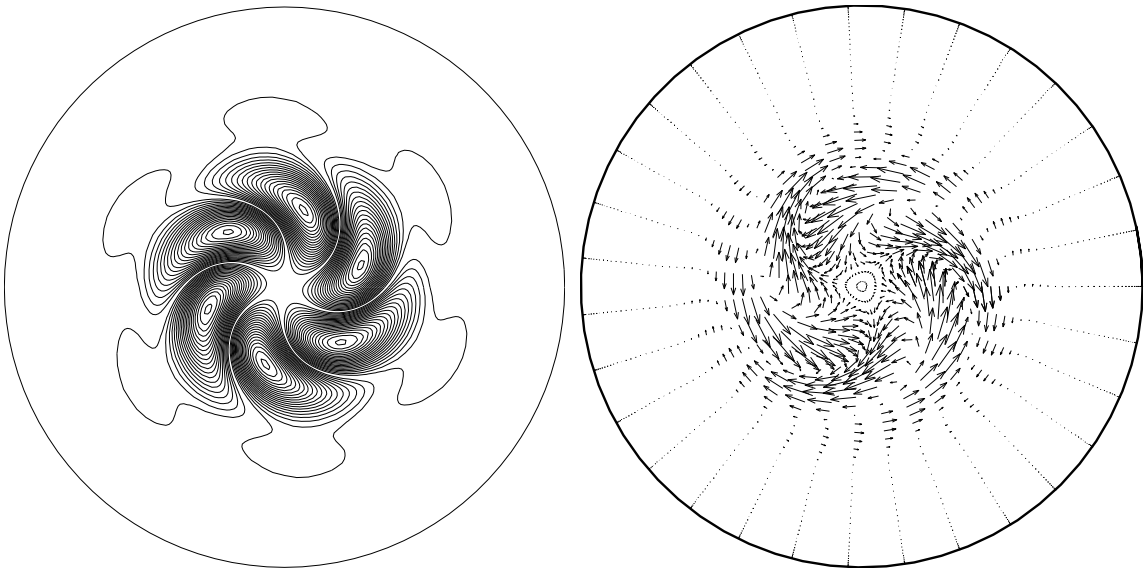

Figure 7: Constant-z cross sections of center-mode stream function and vector field corresponding to the $n = 3$, $k = 1$ least stable eigenvalue $\lambda_1 = -0.08325397694 + 0.86436392104\mathrm{i}$ for $\mathrm{Re} = 3000$.

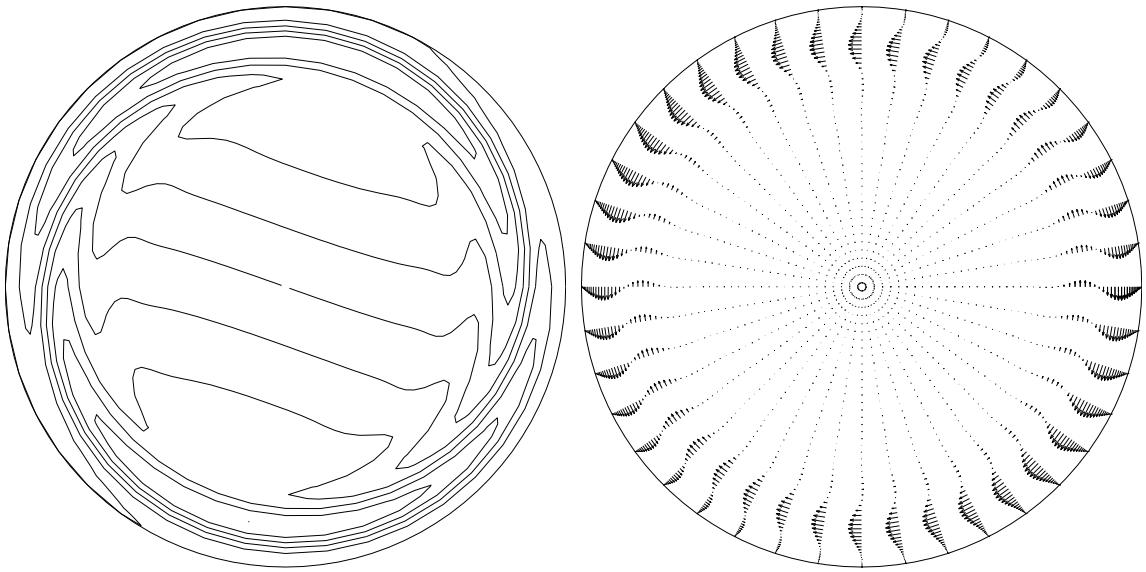

Figure 8: Constant-z cross sections of stream function and vector field corresponding to the $n = 1$, $k = 1$ wall eigenvalue $\lambda_w = -0.1168771535871 + 0.216803862997\mathrm{i}$ for $\mathrm{Re} = 3000$.

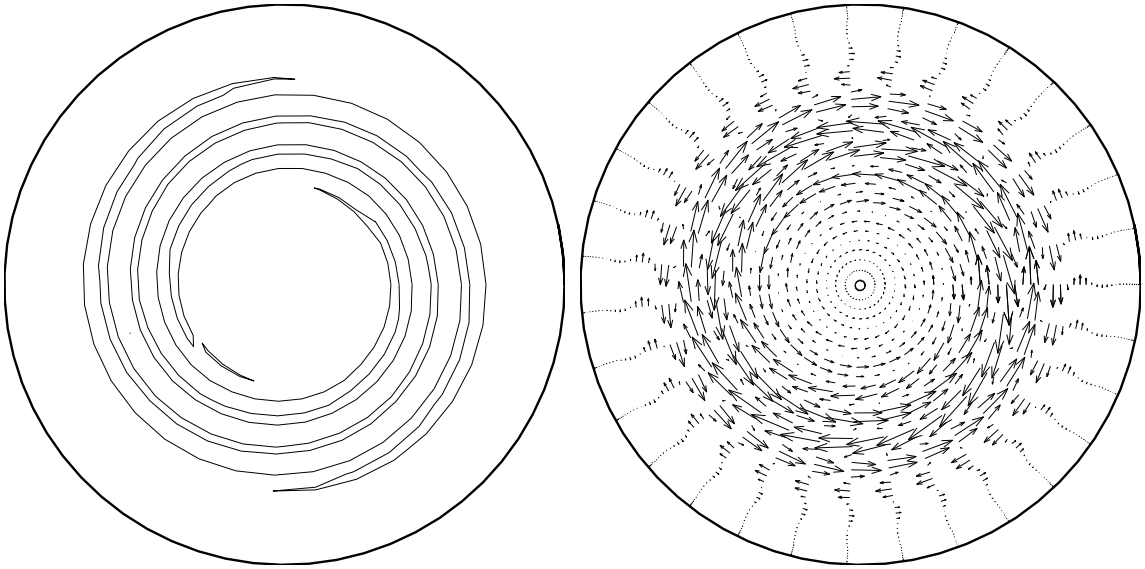

Figure 9: Constant-z cross sections of stream function and vector field corresponding to the $n = 1$, $k = 1$ mean eigenvalue $\lambda_m = -0.414686969578724 - 0.6758740075335031$ for $\mathrm{Re} = 3000$.

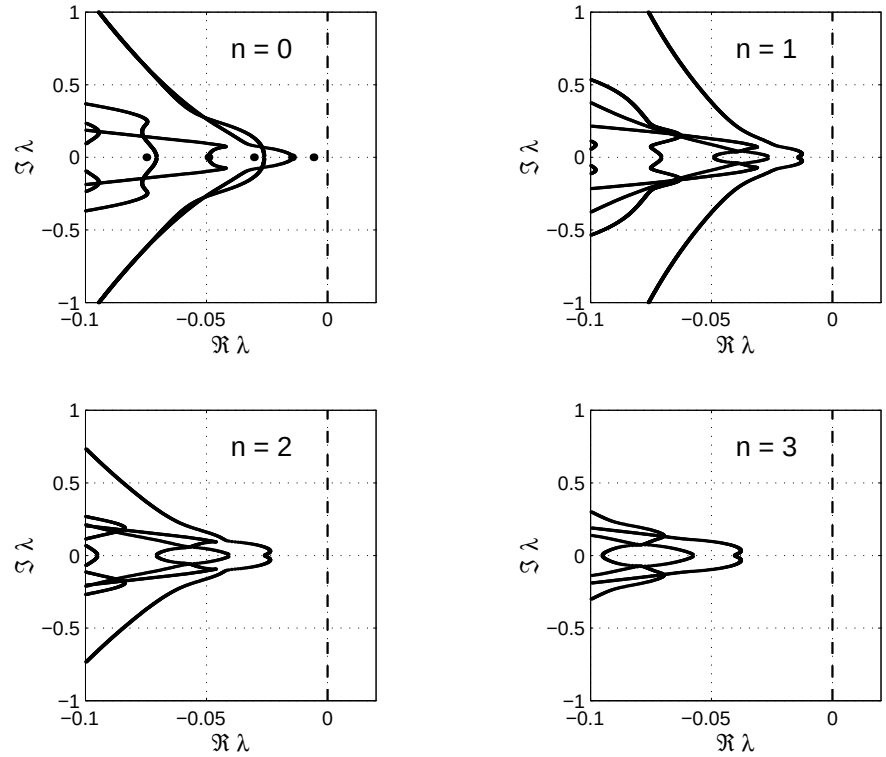

Figure 10: Evolution of the least stable eigenvalues as a function of the axial wavenumber $k \in [0, 1]$. Note the discontinuity of the curves near the real axis for $n = 0$ (top-left), where dots correspond to $k = 0$. Compare (Trefethen *et al.*, 1999). The computation has been done for $\mathrm{Re} = 1000$ and $n = 0, 1, 2, 3$.

4 Pseudospectra and linear transient growth

Although there is no proof, it appears clear from numerical evidence that Hagen-Poiseuille flow is linearly stable under infinitesimal perturbations. Nevertheless, it is experimentally known that it may exhibit transition to turbulent regimes for Re ~ 2000 or higher, see (Darbyshire & Mullin, 1995), for example. Therefore, classical linear hydrodynamic stability theories based on the analysis of eigenvalues do not provide an explanation for the destabilization of the basic flow. We have a so called *subcritical* instability. In other words, there is not any bifurcation but the flow nevertheless becomes unstable. The same behaviour is exhibited by other shear flows like *plane Couette flow*, *plane Poiseuille flow* or *Blasius boundary layer* flow; see (Schmid & Henningson, 1999).

In the past decade, some new theoretical approaches have provided a possible explanation of transition in shear flows. Mathematically, the linear operators arising from shear flow systems present a common feature: *non-normality*. In other words, the operators do not commute with their adjoints, or their eigenvectors are not orthogonal (or far from being orthogonal). Is it a known fact that linearly stable non-normal dynamical systems may exhibit transient growth by many order of magnitude for finite times before eventually decaying exponentially, see (Trefethen *et al.*, 1993), (Butler & Farrell, 1992), (Boberg & Brosa, 1988) or (Gustavsson, 1991).

Although for long times, the behaviour of the linear system is governed by the exponential decay associated with the eigenvalues, for short times, some light can be shed on the dynamical evolution of a linearly stable non-normal system by a generalization of the concept of spectra of operators based on their resolvent norm:

Definition 4.1 *The* ϵ-pseudospectrum *of a matrix* M*, denoted by* $\Lambda_\epsilon(M)$*, is the subset of the complex plane defined by:*

$$\Lambda_\epsilon(M) = \{z \in \mathbb{C} \quad | \quad \|(z\mathrm{I} - M)^{-1}\| \geq \epsilon^{-1}\}.$$

Thus, $\Lambda_\epsilon(M)$ are nested subsets in the complex plane which collapse for $\epsilon = 0$ to the spectrum of M, denoted by

$$\Lambda(M) = \lim_{\epsilon \to 0} \Lambda_\epsilon(M).$$

Potential transient growth can be predicted from the pseudospectra of the operator $M = A^{-1}B_{\mathrm{Re}}$, from the generalized eigenvalue problem (2.61), when considering a suitable energy norm. The energy of an initial perturbation may be amplified transiently if and only if

$$\gamma_\epsilon \doteq \sup_{\epsilon > 0} \frac{\beta(\epsilon)}{\epsilon} > 1, \tag{4.1}$$

where $\beta(\epsilon)$ is the maximum real part of the ϵ-*pseudospectrum*.

Making use of another MATLAB code, see (Trefethen, 1999), we have computed the pseudospectra of the generalized eigenvalue problem through inversion of the matrix A. Plots of spectra and pseudospectra for the cases $(k = 1, n = 0, 1, 2)$ are depicted in figure 11. In all the cases, we projected over the subspace of eigenvalues with real part greater or equal to -2. Plots of spectra and pseudospectra for the cases $(k = 0, n = 0, 1, 2)$ are depicted in figure 12.

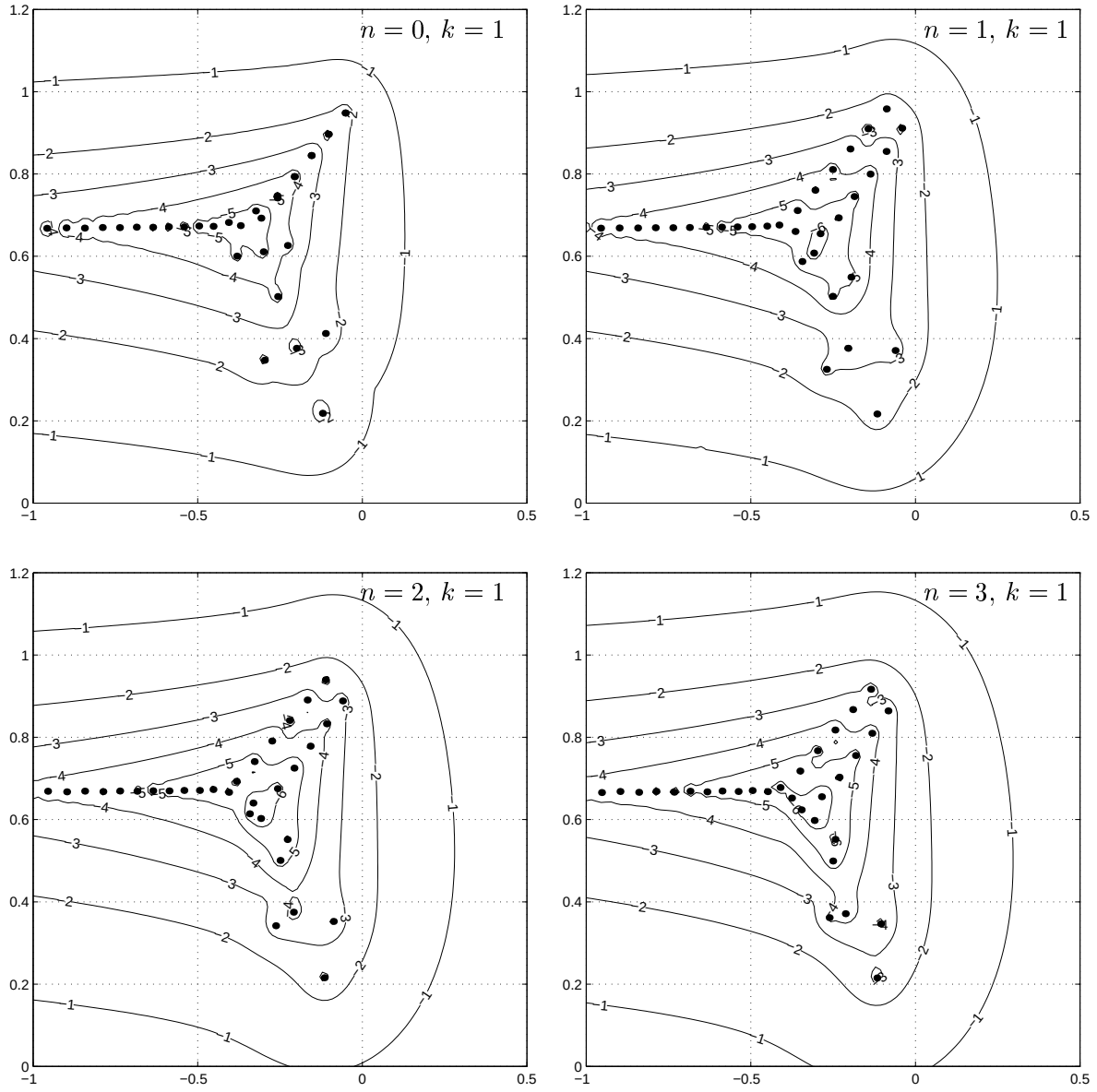

Figure 11: Spectra and pseudospectra for Re = 3000 and $k = 1$. The labels $-0.5,\ -1.0,\ \ldots$ located at the contour levels correspond to the levels $\epsilon = 10^{-1/2},\ \epsilon = 10^{-1}$, etc.

Let us consider a perturbation whose initial density of kinetic energy is $\mathcal{E}(0)$ at $t = 0$. We are interested in the potential transient amplification of this energy for intermediate time scales. Let $\mathcal{E}(t)$ the energy density at time t. We define the *transient factor* $G(t)$ as the quotient

$$G(t) = \frac{\mathcal{E}(t)}{\mathcal{E}(0)}. \tag{4.2}$$

In other words, transient growth occurs when $G(t) > 1$, for small t. Different initial perturbations with the same energy density but different structure will lead to different values of $G(t)$ at time t. We are interested in those initial perturbations which would lead to an *optimal* growth $G_{max}(t)$, see (Butler & Farrell, 1992). This can be understood as a variational problem, where we are maximizing $G(t)$, for a fixed t, with respect to initial conditions. The initial value problem (2.83)

$$\dot{\boldsymbol{\kappa}} = \Lambda \boldsymbol{\kappa}$$

will dictate the linear evolution of an initial condition $\kappa(0)$ through the exponential mapping (2.86)

$$\boldsymbol{\kappa}(t) = \mathrm{e}^{\Lambda t}\boldsymbol{\kappa}(0).$$

The maximum possible amplification $G(t)$ of energy at time t will be given by

$$G_{max}(t) = \sup_{||\boldsymbol{\kappa}(0)||\neq 0} \frac{||\boldsymbol{\kappa}(t)||^2}{||\boldsymbol{\kappa}(0)||^2} = ||\mathrm{e}^{\Lambda t}||^2_{\mathcal{E}} = ||\mathcal{F}\mathrm{e}^{\Lambda t}\mathcal{F}^{-1}||^2_2 \tag{4.3}$$

The singular value decomposition (SVD) provides the vectors $\boldsymbol{\kappa}(0)$ (*right singular vectors*) which maximize the norm of $\boldsymbol{\kappa}(t)$ (*left singular vectors*); see (Trefethen & Bau, 1997). We have used the SVD to compute the right singular vectors which maximize the energy norm (kinetic energy density). Thus, $G_{max}(t)$ is the maximum transient factor obtained from the SVD analysis.

From figure 12b, we can estimate a lower bound for the maximum energy transient G_{max}. The quantity γ_ϵ provides a lower bound for the maximum possible growth G_{max}

$$G_{max} \geq \gamma_\epsilon^2,$$

see (Trefethen, 1992). Thus, for example, in figure 12b the $\epsilon = 1/\sqrt{10}-$pseudospectrum (contour label -0.5) protrudes into the real positive complex plane achieving a maximum value $\beta(\epsilon) \sim 1/2$. This implies a transient growth of at least $G_{max} = (\beta(\epsilon)/\epsilon)^2 = (\sqrt{10}/2)^2 = 5/2$. In figure 13, we have plotted the energy transients corresponding to two particular eigenmodes for $\mathrm{Re} = 3000$. Our results agree with previous computations (Schmid & Henningson, 1994). We have carried out a comprehensive exploration of the transient growth in the (R, k, n) parameter space. The numerical results have been compiled in figure 14. For this exploration, we have considered a range of values of R from 10^2 to 10^5, azimuthal numbers $n = 0, 1, 2, 3$ and axial wave numbers $k = 0, 0.1, 1, 10$. Finally, we have simulated the time evolution of a localized perturbation via the linearized dynamical system of amplitudes for $\mathrm{Re} = 1000$. In figure 15, we have plotted the constant-$||\mathbf{v}||$ surface of a localized vortex in the interval $z \in [5, 6]$ at $t = 0$ (top). After a transient time $t = 10$, the perturbation has been advected downstream a distance $\Delta z \sim 10$ and it has grown in size. For $t = 40$ the structure appears even more elongated at the beginning of the periodic pipe (the whole structure has already completed a periodic cycle in the axial coordinate). The eventual decay of the size of the perturbation can be observed at $t = 50$ (bottom).

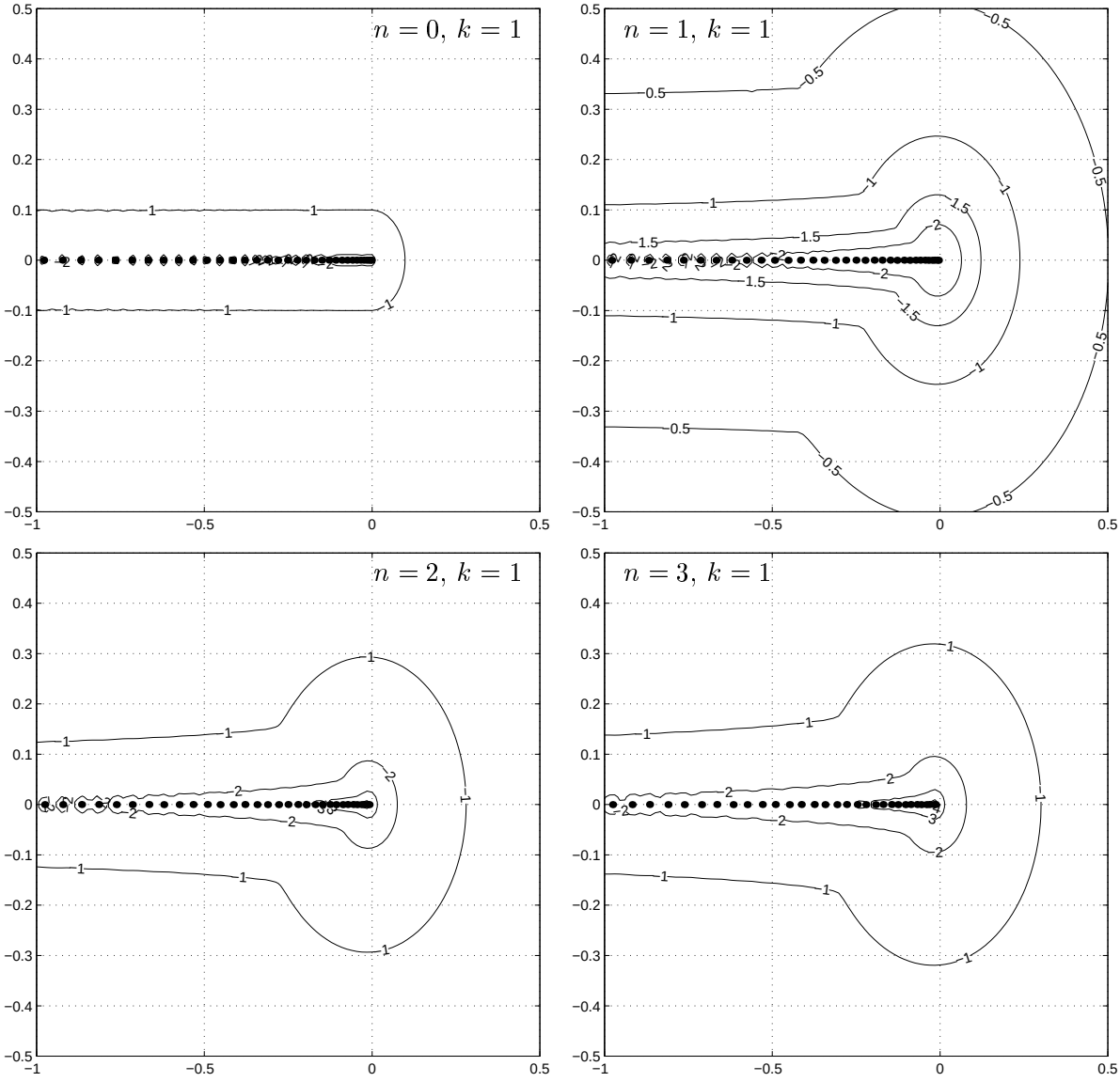

Figure 12: Spectra and pseudospectra for $\mathrm{Re} = 3000$, now for $k = 0$.

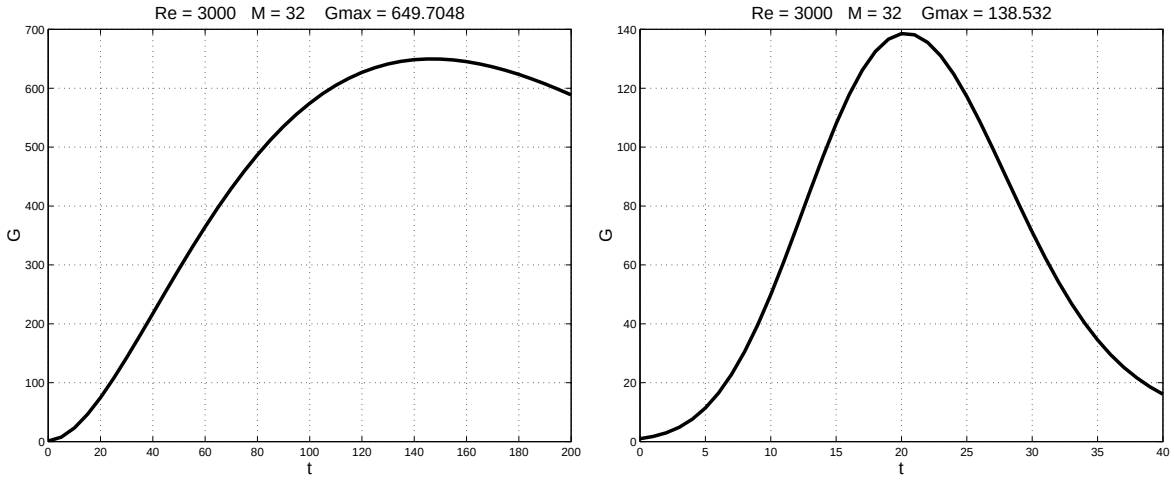

Figure 13: Transient optimal growth for $k = 0$, $n = 1$ (left) and $k = 1$, $n = 1$ (right), following (Schmid & Henningson, 1994). The computation has been done for Re = 3000.

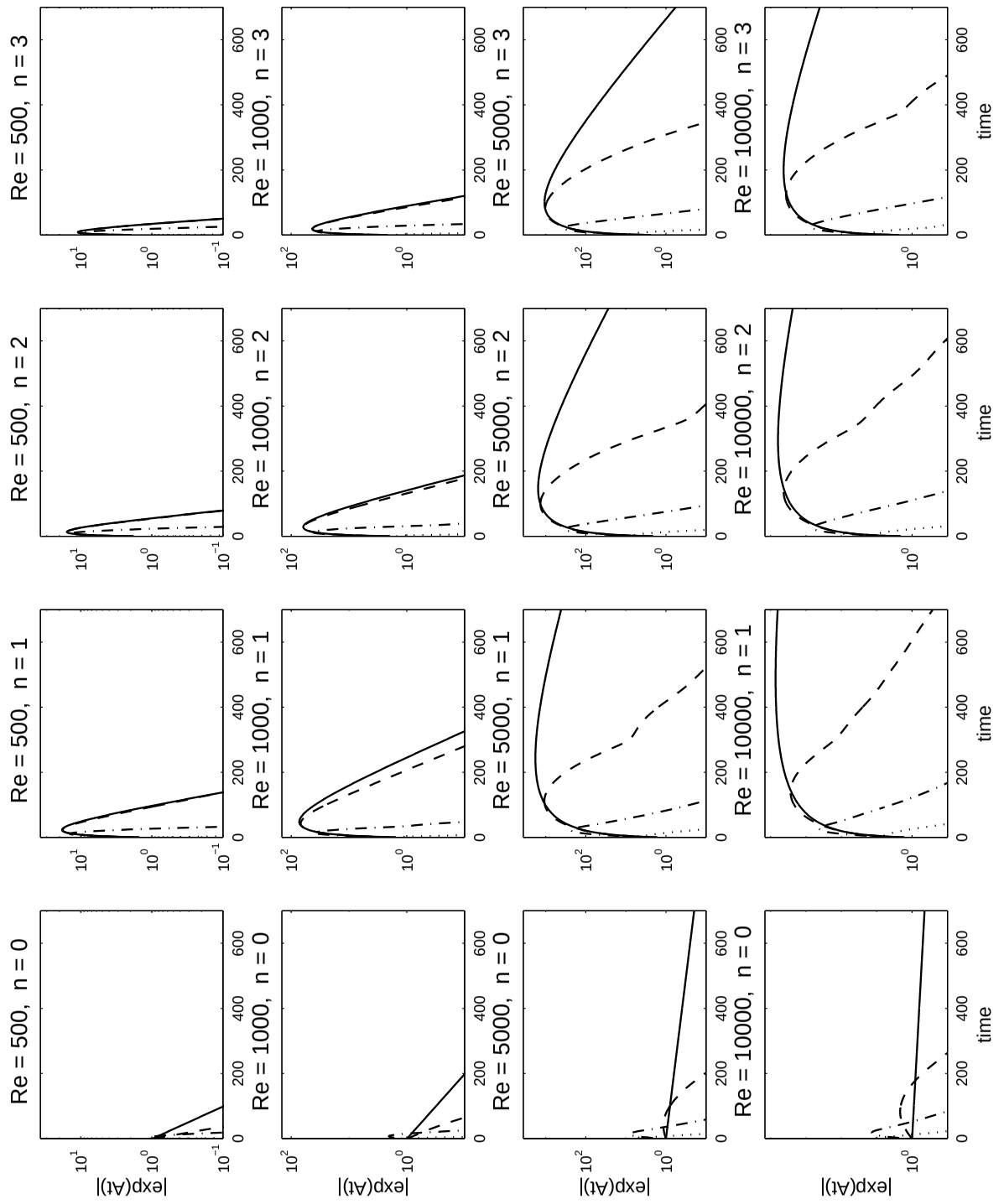

Figure 14: Transient optimal growth G_{max}. Exploration for different values of R, k and n. The solid line denotes $k = 0$, the dashed line $k = 0.1$, the chain-dashed $k = 1$ and the dotted line $k = 10$.

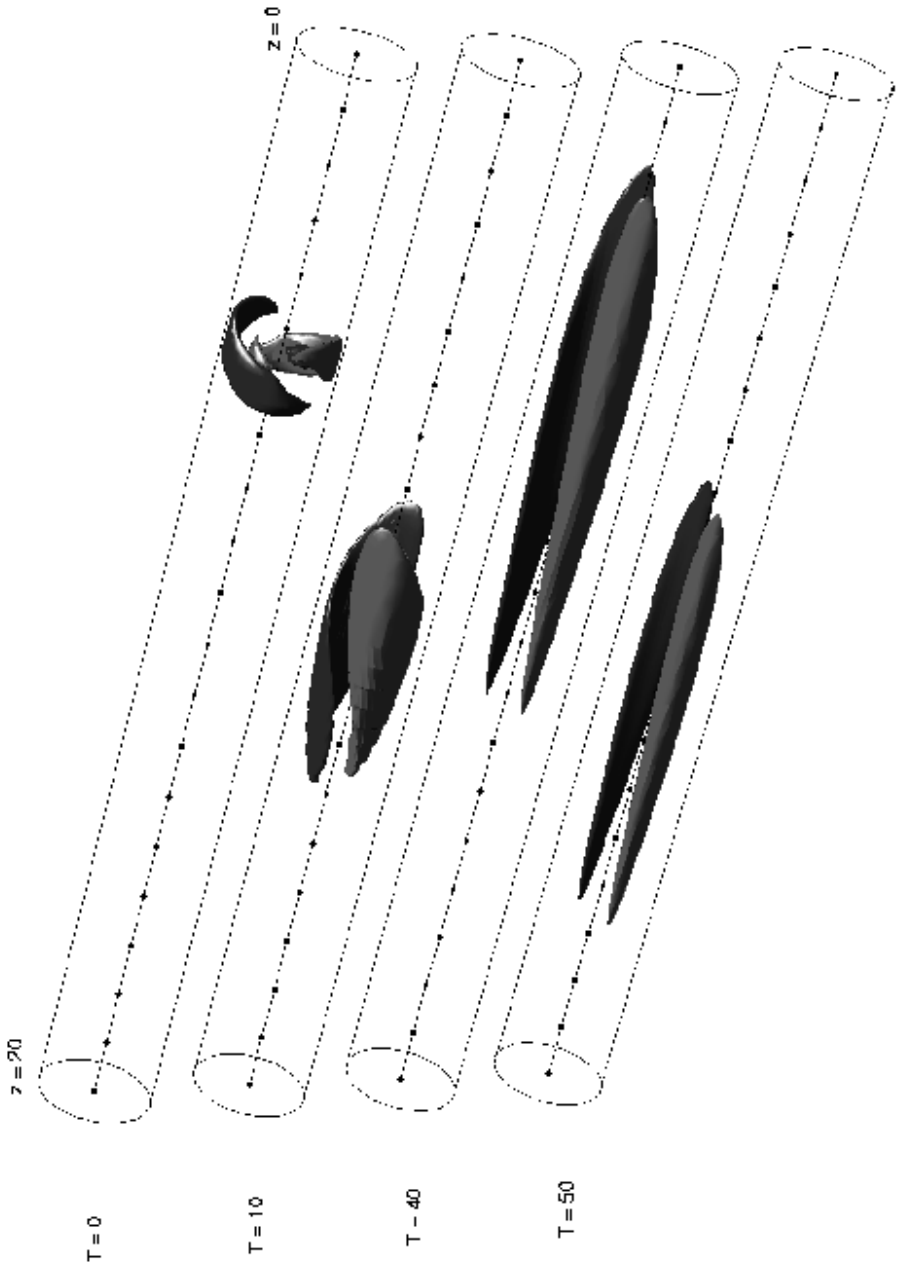

Figure 15: Transient growth of a localized perturbation for Re = 1000.

5 Appendix: Matlab codes

```
function [r,L,A,B] = pipe11(Re,n,k,M)

%  ************************************************************
%  ********      Spectral code for stability analysis      ********
%  ********          of ideal circular pipe flow           ********
%  ********      (solenoidal Petrov-Galerkin approach)     ********
%  ********                                                ********
%  ********         A. Meseguer  &  L. N. Trefethen        ********
%  ********                                                ********
%  ********                   Version 11                   ********
%  ********                                                ********
%  ********             Oxford  -  February 2000           ********
%  ************************************************************

% Parameters
%
% Re = Reynolds number
% n  = azimuthal wavenumber
% k  = axial wavenumber
% M  = number of Chebyshev modes for spectral approximation
%
% Variables
%
%       N = number of points for Chebyshev-Gauss-Lobatto quadrature (odd)
%      rr = Chebyshev grid for radial variable in [-1,1]
%       r = restriction of rr to [0,1)
%      r2 = r^2
%       w = Gauss quadrature weights corresponding to grid r
%      hp = Hagen-Poiseuille basic flow
%     dhp = first radial derivative of hp
%    D,D2 = Chebyshev differentiation matrix and its square
%  DE,D2E = even halves of D and D2
%  DO,D2O = odd halves of D and D2
%     G,H = Chebyshev polynomials (1-r^2)^2 T_2m(r), (1-r^2) T_2m(r)
%
% External functions
%
% vprj = generate vector basis V of spectral approximation
% vbas = generate vector basis VP of test projection

% Global variables and indices

  global DO DE
  M1 = M+1; N = 2*M+2*abs(n)+9;
  K = (N-1)/2;      % number of grid points in [0,1)
```

```
  half = K+2:N;     % indices of grid points in [0,1)
  rad = 1:K;        % indices of radial components
  az = K + rad;     % indices of azimuthal components
  ax = K + az;      % indices of axial components

% Chebyshev mesh and differentiation matrix for rr in [-1,1]

  rr = cos(pi*(0:N)/N)';
  c = [2; ones(N-1,1); 2].*(-1).^(0:N)';
  X = repmat(rr,1,N+1);
  dX = X-X';
  D  = (c*(1./c)')./(dX+(eye(N+1)));      % off-diagonal entries
  D  = D - diag(sum(D'));                 % diagonal entries

% Extraction from D and its square of pieces for r in [0,1]

  D2 = D^2;
  DE = D(half,half) + D(half,N+2-half);
  DO = D(half,half) - D(half,N+2-half);
  D2E = D2(half,half) + D2(half,N+2-half);
  D2O = D2(half,half) - D2(half,N+2-half);
  clear D D2
  r = rr(half); r2 = r.^2;
  w = ones(size(r))'*pi/N;
  hp = Re*(r.^2-1); dhp = 2*Re*r;

% OUTLINE OF PETROV-GALERKIN PROCEDURE
%
% Define LNS = linearized Navier Stokes operator D2-(n^2)/r^2-....
% (For explicit expressions see Appendix C of Meseguer's thesis.)
%
% Evolution equation:
%   v_t = LNS[v] + pressure term, which cancels in the projection
%
% Eigenmode solution:
%     v = v(r) exp(i( k*z + n*theta)) exp(lambda*t)
%
% Formulation as generalized eigenvalue problem:
%     A lambda v = B v,  A = (VP,V) ,  B = (VP,LNS[V])
%
% Inner product: (f,g) = integral of f*(r) g(r) r dr  over [0,1]

% Sparse diagonal scaling matrices

  nka = (n^2+1)./r+(k^2+i*k*hp).*r; nkb = nka-1./r;
  NK = spdiags([nka; nka; nkb],0,3*length(nka),3*length(nka));
```

```
  W = spdiags([w'; w'; w'],0,3*length(w),3*length(w));
  R = spdiags([r; r; r],0,3*length(r),3*length(r));
  Ri = spdiags([1./r; 1./r],0,2*length(r),2*length(r));
  WDHPR = spdiags(w'.*dhp.*r,0,length(r),length(r));

% Computation of vector fields

  G  = zeros(K,M1); H  = zeros(K,M1); V  = zeros(3*K,2*M1);
  VP = zeros(2*M1,3*K); LV = zeros(3*K,2*M1);
  for m = 1:M1
    H = (1-r2).*cos(2*(m-1)*acos(r));
    G = (1-r2).*H;
    pair = [m m+M1];
    VP(pair,:) = vprj(n,k,r,G,H);
    V(:,pair)  = vbas(n,k,r,G,H);
  end
  if rem(n,2)==0       % n even
    for m = 1:M1
      pair = [m m+M1];
      LV(:,pair) = R*[D2O*V(rad,pair);D2O*V(az,pair);D2E*V(ax,pair)] ...
                   + [DO*V(rad,pair); DO*V(az,pair); DE*V(ax,pair)] ...
                   - NK*V(:,pair);
    end
  else                 % n odd
    for m = 1:M1
      pair = [m m+M1];
      LV(:,pair) = R*[D2E*V(rad,pair);D2E*V(az,pair);D2O*V(ax,pair)] ...
                   + [DE*V(rad,pair); DE*V(az,pair); DO*V(ax,pair)] ...
                   - NK*V(:,pair);
    end
  end

% Computation of matrices A, B, and L

  A = VP*(W*R)*V;
  B = VP*W*LV - VP(:,ax)*WDHPR*V(rad,:) ...
       + 2i*n*([VP(:,az) -VP(:,rad)]*W([az rad],[az rad]) ...
          *Ri*[V(rad,:);V(az,:)]);
  clear D2E D2O WDHPR LV VP V W R Ri DE DO
  L = (A\B)/Re;
```

```
function v = vbas(n,k,r,G,H)

% VBAS  Spectral basis (two column vectors)

  global DE DO
  z = zeros(size(r));
  an = abs(n);


  if n==0
    if k==0
      v1r=z;                  v1t=r.*H;              v1z=z;
      v2r=z;                  v2t=z;                 v2z=H;
    else
      v1r=z;                  v1t=r.*H;              v1z=z;
      v2r=-i*k*r.*G;          v2t=z;                 v2z=DO*(r.*G)+G;
    end
  elseif rem(n,2)==0

    if k==0
      v1r=-i*n*G.*r.^(an-1); v1t=DE*(r.^an.*G);     v1z=z;
      v2r=z;                  v2t=z;                 v2z=r.^an.*H;
    else
      v1r=-i*n*G.*r.^(an-1); v1t=DE*(r.^an.*G);     v1z=z;
      v2r=z;                  v2t=-r.^(an+1).*H*k;   v2z=r.^an.*H*n;
    end
  else

    if k==0
      v1r=-i*n*G.*r.^(an-1); v1t=DO*(r.^an.*G);     v1z=z;
      v2r=z;                  v2t=z;                 v2z=r.^an.*H;
    else
      v1r=-i*n*G.*r.^(an-1); v1t=DO*(r.^an.*G);     v1z=z;
      v2r=z;                  v2t=-r.^(an+1).*H*k;   v2z=r.^an.*H*n;
    end
  end

  v = [v1r v2r; v1t v2t; v1z v2z];
```

```
function v = vprj(n,k,r,G,H)

% VPRJ  Test basis (two row vectors, already conjugated)

  global DE DO
  z = zeros(size(r));

% n = 0
  if n==0
    if k == 0
      v1r=z;             v1t=H;                      v1z=z;
      v2r=z;             v2t=z;                      v2z=r.*H;
    else
      v1r=z;             v1t=H;                      v1z=z;
      v2r=i*k*r.^2.*G;   v2t=z;       v2z=DE*(r.^2.*G)+r.^3.*H+r.*G;
    end
  end

% n = 2,4,6,...
  if n~=0 & rem(n,2)==0
    if k == 0
      v1r=i*n*G;         v1t=DO*(r.*G)+r.^2.*H;     v1z=z;
      v2r=z;             v2t=z;                      v2z=r.*H;
    else
      v1r=i*n*G;         v1t=DO*(G.*r)+r.^2.*H;     v1z=z;
      v2r=z;             v2t=-r.^2.*H*k;             v2z=r.^1.*H*n;
    end
  end

% n = 1,3,5,...
  if rem(n,2)~=0
    if k==0
      v1r=i*n*G.*r;      v1t=DE*(r.^2.*G)+r.^3.*H; v1z=z;
      v2r=z;             v2t=z;                      v2z=H;
    else
      v1r=i*n*G.*r;
      v1t=DE*(G.*r.^2)+r.^3.*H;
      v1z=z;
      v2r=z;             v2t=-r.^3.*H*k;             v2z=r.^2.*H*n;
    end
  end

  v = [v1r v2r; v1t v2t; v1z v2z].';
```

Acknowledgments

This research was supported by the Engineering and Physical Sciences Research Council of the UK under Grant GR/M30890.

References

J. S. Baggett and L. N. Trefethen. *Low-dimensional models of subcritical transition to turbulence.* Phys. Fluids **9**(4), (1997).

G. K. Batchelor. *An Introduction to Fluid Dynamics.* Cambridge University Press (1967).

J. P. Boyd. *Chebyshev and Fourier Spectral Methods.* Dover (1999).

L. Boberg and U. Brosa. Z. Naturforsch., A: Phys. Sci. **43**, 697 (1988).

K. M. Butler and B. F. Farrell. *Three-dimensional optimal perturbations in viscous shear flow.* Phys. Fluids A **4**(8) (1992).

C. Canuto, M.Y. Hussaini, A. Quarteroni, T.A. Zang. *Spectral Methods in Fluid Dynamics.* Springer-Verlag (Springer Series in Computational Physics) (1988).

A. G. Darbyshire & T. Mullin. *Transition to turbulence in constant-mass-flux pipe flow.* J. Fluid Mech. **289**, 83-114 (1995).

P. G. Drazin and W. H. Reid. *Hydrodynamic Stability.* Cambridge Univ. Press, 1981.

L. H. Gustavsson. *Energy growth of three dimensional disturbances in plane Poiseuille flow.* J. Fluid Mech. **224**, 241 (1991).

D. D. Joseph. *Stability of Fluid Motions* vol. I and II. Springer Tracts in Natural Philosophy, 27-28. Springer-Verlag, Berlin (1976).

A. Leonard and A. Wray. *A new numerical method for the simulation of three dimensional flow in a pipe.* Proceedings, 8th Int. Conf. on Numerical Methods in Fluid Dynamics, ed. E. Krause (Springer-Verlag, Berlin, 1982).

A. Meseguer. *Bifurcations in Fluid Systems: Petrov-Galerkin Schemes.*. PhD Thesis. Universitat Politècnica de Catalunya, Barcelona (1998).

R.D. Moser, P. Moin, A. Leonard. *A spectral numerical method for the Navier-Stokes equations with applications to Taylor-Couette Flow.* J. Comput. Phys. **52**, 524-544 (1983).

V. G. Priymak and T. Miyazaki. *Accurate Navier-Stokes Investigation of Transitional and Turbulent Flows in a Circular Pipe.*. Jour. of Comp. Phys. **142**, 370–411 (1998).

P. J. Schmid and D. S. Henningson. *Optimal energy growth in Hagen-Poiseuille flow.* J. Fluid Mech., vol. 277, pp. 197-225 (1994).

P. J. Schmid and D. S. Henningson. *Stability and Transition in Shear Flows.* To appear.

L. N. Trefethen *Pseudospectra of matrices.* Numerical Analysis (ed. D. F. Griffiths and G. A. Watson). Longman (1992).

L. N. Trefethen and D. Bau. *Numerical Linear Algebra.* SIAM (1997).

L. N. Trefethen, A. E. Trefethen, S. C. Reddy and T. A. Driscoll *Hydrodynamic Stability Without Eigenvalues.* Science. **261** (1993).

A. E. Trefethen, L. N. Trefethen and P.J. Schmid. *Spectra and pseudospectra for pipe Poiseuille flow.* Comp. Meth. Appl. Mech. Engr. (1999).

L. N. Trefethen. *Computation of Pseudospectra.* Acta Numerica (1999).